Polytriazole membranes with ultrathin tunable selective layer for crude oil fractionation

Item Type	Article
Authors	Chisca, Stefan; Musteata, Valentina-Elena; Zhang, Wen; Vasylevskyi, Serhii; Falca, Gheorghe; Abou-Hamad, Edy; Emwas, Abdul-Hamid M.; Altunkaya, Mustafa; Nunes, Suzana Pereira
Citation	Chisca, S., Musteata, V.-E., Zhang, W., Vasylevskyi, S., Falca, G., Abou-Hamad, E., Emwas, A.-H., Altunkaya, M., & Nunes, S. P. (2022). Polytriazole membranes with ultrathin tunable selective layer for crude oil fractionation. Science, 376(6597), 1105–1110. https://doi.org/10.1126/science.abm7686
Eprint version	Post-print
DOI	10.1126/science.abm7686
Publisher	American Association for the Advancement of Science (AAAS)
Journal	Science
Rights	Archived with thanks to Science
Download date	18/09/2023 13:25:17
Link to Item	http://hdl.handle.net/10754/678595

Polytriazole membranes with ultrathin tunable selective layer for crude oil fractionation

Stefan Chisca[1,2], Valentina-Elena Musteata[1,3], Wen Zhang[3†], Serhii Vasylevskyi[3], Gheorghe Falca[1,2], Edy Abou-Hamad[3], Abdul-Hamid Emwas[3], Mustafa Altunkaya[3], Suzana P. Nunes[1,2,4,5*]

[1]Environmental Science and Engineering Program, Biological and Environmental Science and Engineering Division (BESE), King Abdullah University of Science and Technology (KAUST), , Thuwal, Saudi Arabia

[2]Advanced Membranes and Porous Materials (AMPM) Center, King Abdullah University of Science and Technology (KAUST)

[3]Core Labs, King Abdullah University of Science and Technology (KAUST),

[4]Chemical Science Program, Physical Science and Engineering Division (BESE), King Abdullah University of Science and Technology (KAUST)

[5]Chemical Engineering Program, Physical Science and Engineering Division (BESE), King Abdullah University of Science and Technology (KAUST)

*Corresponding author. Email: suzana.nunes@kaust.edu.sa

†Present address: Dept. Environmental Science, Stockholm University, 106 91 Stockholm, Sweden

Abstract The design of materials and their manufacture into membranes that can handle industrial conditions and separate complex non-aqueous mixtures are challenging. We report a versatile strategy to fabricate polytriazole membranes with 10 nm thin selective layers containing subnanometer channels for the separation of hydrocarbons. The process involves the use of the classical non-solvent induced phase separation method and thermal crosslinking. The membrane selectivity can be tuned to the lower end of the typical nanofiltration range (200 to 1000 g mol^{-1}). The polytriazole membrane can enrich up to 80-95 % of the hydrocarbon content with less than 10 carbon atoms (140 g mol^{-1}). These membranes preferentially separate paraffin over aromatic components, making them suitable for integration in hybrid distillation systems for crude oil fractionation.

One-Sentence Summary: Crosslinked polytriazole nanofiltration polymeric membranes for crude oil fractionation

Separation processes are essential in the chemical, pharmaceutical, and petrochemical industries and are widely used to purify solvents and chemicals, solvent exchange, catalyst recycle and recovery (*1*). Conventional separation techniques such as distillation, adsorption, evaporation, and extraction are energy-intensive. These separations represent up to 40–70% of both capital and operating costs (*2*).

Membrane technology is considered sustainable due to its low carbon footprint, small spatial requirements, and a lack of phase transition in most cases. Organic solvent nanofiltration (OSN) could more broadly replace traditional separation processes (*3*) if better membranes address the requirements of chemical, pharmaceutical, and petrochemical processes (*4*). For that, the membranes should combine easy processability with stability in a wide range of organic solvents and pH. They should be mechanically and thermally stable to reduce the physical aging since many processes in the chemical, pharmaceutical, and petrochemical separations take place at 60–90 °C or even higher temperature ranges (*5-7*). Although inorganic materials might have higher thermal and solvent stability, they have limitations, such as high cost, low mechanical properties, and difficult scale-up (*8*).

Polymeric membranes are less expensive than most inorganic ones, easy to process and integrate in large-scale modules. However, only a few classes of polymeric materials, such as poly(dimethylsiloxane) and polyimide, are being industrially used for nanofiltration of non-aqueous solutions. Polybenzimidazole, poly(ether ether ketone), and polymers with intrinsic microporosity (PIM) are under evaluation (*9-11*). Swelling effects, when exposed to harsh environments, affect the separation performance in many cases. Recently, a series of PIM-like polymers was reported that show attractive crude oil separations (*12*). This is a challenging separation and more materials are needed to handle the industrial conditions and successfully separate complex mixtures (*13*). Overcoming the permeability and selectivity trade-off, particularly in industries like crude oil refining (*5, 13*) without considerable membrane aging is a difficult task.

We report a simple strategy to fabricate polytriazole asymmetric membranes with ultrathin selective layers by combining the classical non-solvent induced phase separation (NIPS) method and thermal crosslinking. The resulting membranes were tested with highly challenging liquid feeds containing high-boiling polar aprotic solvents used to extract aromatic fractions from refinery streams, and separately tested with one of the most complex mixtures like those present in crude oil. We chose polytriazole with pendant hydroxyl (OH) groups (PTA-OH, Fig. 1A, characterized in Figs. S1-S3)(*14*) as membrane material because it can easily be synthesized in large quantity with good mechanical properties and has a high thermal and thermal-oxidative stability. Additionally, the pendant OH groups make this polymer versatile in terms of crosslinking or modification (*14*). The membrane formation first involves the dissolution of the polytriazole polymer in the solvents (N-methyl-2-pyrrolidone (NMP) or N,N′-dimethylformamide (DMF)), followed by solution casting and immersion in water. To induce the crosslinked reaction, we simply treated the polytriazole membranes at 300°C for 1h, 2h and 3h, and at 325°C for 1h and 2h, in a furnace under an air environment. The resulting crosslinked membranes are stable in organic solvents, in strong acids (hydrochloric acid 37% (HCl) and sulfuric acid 98% (H_2SO_4)) and base (sodium hydroxide 2M (NaOH)) (Fig. S4). A PTA (without OH) membrane treated at 325°C for 2h dissolved in tetrahydrofuran, indicating that the the OH functionalization is relevant for the crosslinking reaction.

We propose that the PTA-OH thermal crosslinking leads to the structure depicted in Fig. 1A. To confirm it, we applied Fourier Transform Infrared (FTIR) spectroscopy, high-resolution Solid-State Nuclear Magnetic Resonance (SS-NMR), Dynamic Nuclear Polarization (DNP) coupled with multinuclear 2D (^{1}H, ^{13}C, ^{17}O, ^{15}N) spectroscopy, and Electron Paramagnetic Resonance (EPR) spectroscopy. The spectra are shown in Figs. 1B-D and Figs. S5-S11.

FTIR (Fig. S5) did not show significative change, besides a slight decrease of the broad peak characteristic of OH, indicating that OH remains part of the network. An indication of the crosslinked structure is given by Electron Paramagnetic Resonance (EPR, Fig. S6). While no signal is seen for PTA, the signal characteristic of delocalized electrons for PTA-OH increases as the reaction time for polyoxadiazole to PTA-OH increases. An intenser signal is observed as the membranes are thermally treated, suggesting an increase in carbon conjugation as previously observed in other network forming systems (15). Clearer evidence for the crosslinked structure proposed in Fig. 1 was obtained by SS-NMR and DNP.

The ^{13}C cross-polarization magic-angle spinning (CP-MAS) for the pristine PTA-OH shows the aromatic carbons (Ar) in the region 129-134 ppm, two peaks at 158 and 154 ppm corresponding to chemical shifts for the C – O bond (labeled *a*) and the carbon in the triazole ring (labeled *b*) respectively and a peak at 115 ppm (labeled *c*) (Fig. S7A). For the crosslinked membrane treated at 325°C for 2h a new peak appeared at 155 ppm (labeled *e'*), and additional peaks in the range of 117 - 119 ppm (labeled *e*), which are associated with the formation of the crosslinked network (Fig. S7B). To confirm the findings from CP-MAS data, we used heteronuclear correlation spectroscopy (HETCOR). Fig. 1B compares the 2D ^{1}H-^{13}C and 2D ^{13}C-^{13}C spectra. We used the 2D ^{13}C-^{13}C mixing with proton-driven spin-diffusion (PDSD) and applying phase-alternated-recoupling-irradiation-schemes (PARIS) for 120 ms (CP). This technique provides high resolution and all broad signals can be resolved. In addition to the carbon atoms correlations for the pristine PTA-OH, clear new correlations peaks are presented for the thermally treated membrane at 155, 117, and 119 ppm corresponding to the crosslinked network formation. Moreover, a correlation between carbons participating in the crosslinking and the purely aromatic ones at 129 ppm was detected, indicating that the two carbons are in close physical proximity. A new OH proton was confirmed for the thermally treated membranes by the presence of a new signal at 2.4 ppm in the ^{1}H MAS NMR spectrum (Fig. S8A). Additionally, the 2D ^{1}H-^{1}H double quantum/single quantum displays an extra correlation outside the diagonal between OH and aromatic protons for the thermally treated membranes (Figs. S8B and S8C).

We distinguished two sets of oxygen coordinations (labeled O_1 and O_2) for the thermally treated sample demonstrated by ^{17}O DNP spectroscopy, which offers very high sensitivity, without using isotopically enhanced samples (Fig. 1C Fig. S9). O_1 corresponds to uncrosslinked sites and O_2 to those crosslinked labeled as 2 in Fig. 1A. We also consider a third possibility labeled 3 in Fig. 1A, but its signal would overlap with the others. The successful acquisition of ^{17}O DNP allows us to collect the multidimensional correlation spectroscopy. A major challenge for this analysis has been so far the low natural isotopic (NA=0.038%) and quadrupolar nature of ^{17}O nuclei (I=5/2), which lead to an excessive spectrum line broadening. However, a significant improvement to the application of DNP MAS NMR to ^{17}O has been possible by using the PRESTO polarization transfer technique combined with quadrupolar a Carr-Purcell-Meiboom-Gill (QCPMG) experiment. This enabled us the detection of ^{17}O sites. Fig. S10 shows that the ^{17}O signal of the PTA-OH sample is mostly correlated with OH protons signals, whereas for the thermally treated sample, it is clear that the two different ^{17}O sites are connected with ^{1}H signal of OH and aromatic in agreement with the expected shifts. At the same time, the ^{15}N CP-MAS and the ^{15}N–^{1}H CP-MAS HETCOR of the thermally treated membranes reveal a distribution of new signals in the range of 380-390 ppm attributed to the nitrogen atoms named N_4, N_5 (Fig. 1D Fig. S11).

129   Fig. S12 indicates that by heating a non previously treated PTA-OH membrane only a
130   slight weight decrease (<4%) is observed in the range of 275 - 400°C. For previously treated
131   samples (325°C for 2h) the weight decrease goes down to 1.5 %. PTA (without OH) membranes
132   do not have any loss in this temperature range. This confirms that any reaction in the 275 - 400°C
133   range should involve the OH groups, however with a very low degree of elimination of OH or
134   other groups. TGA analysis coupled with mass spectrometry (TGA-MS) (Fig. S12C) confirmed
135   the low weight loss in this temperature range and indicated that species being eliminated have a
136   mass corresponding to the size of water molecules.
137   In summary, the spectroscopic and thermal analysis characterizations support the structure
138   proposed in Fig. 1A.
139   After the thermal crosslinking, the membranes maintain their flexibility (Fig. S4).
140   Flexibility and minimal plastic deformation are important in pressure-driven membrane
141   applications to ensure that the membrane performance would be maintained for a long time (*5, 6*).
142   The mechanical properties were quantitatively evaluated by dynamic mechanical analysis. The
143   tensile strength and Young's moduli were measured from stress-strain experiments. All
144   membranes exhibited similar stress-strain behavior, but the crosslinked ones have higher values of
145   stress and Young's modulus (Fig. S13). The creep recovery measurement indicates how much the
146   membranes would irreversibly deform under pressure (Fig. S13F). The crosslinked membranes
147   have less pronounced creep, implying that they are less susceptible to irreversible deformation
148   (*16*).
149   Scanning Electron Microscopy (SEM) and Transmission Electron Microscopy (TEM)
150   were used to investigate the morphology of the membranes before and after crosslinking. We
151   compared the SEM images of PTA-OH membranes prepared by the NIPS process from casting
152   solutions in NMP and DMF. In both cases, the untreated membranes have high pore density, but
153   those prepared with NMP have slightly smaller pores and lower porosity seen in surface (Fig. S14)
154   and cross-sectional images (Fig. 2 and Fig. S15). As a consequence, the water permeance is higher
155   for the membranes prepared with DMF (90 L h m^2 bar^{-1}) compared with those using NMP (60 L
156   h m^2 bar^{-1}), while the molecular weight cutoff is 25 kg mol^{-1} and 10 kg mol^{-1}, respectively. The
157   SEM images reveal that the thermal treatment induces a relaxation of the surface polymer layer,
158   closing the pores, and forming an ultrathin dense layer on the top of the membrane (Fig. 2). This
159   denser layer can be better seen by TEM (Fig. 2E-G, S16 and S17). What appears to be scattered
160   pinholes on the surface can be still identified in the D300-2h membrane (Fig. S14A), but
161   membranes treated at higher temperatures have a defect-free surface. The TEM image of a D300-
162   1h membrane in Fig. S16A shows pores partially closed while the dense layer is being formed.
163   Membranes cast from NMP are pinhole-free even when treated at 300°C. Their dense layer is
164   smoother and thinner. The wavy morphology of the denser layer of membranes cast from DMF
165   originates due to the larger pores of the pristine membranes. Although the polytriazole Tg is above
166   350°C (Fig. S12D), the polymer chain mobility close to the surface can be higher than in the bulk
167   as reported for other glassy systems (*17*) and leads to the formation of the dense ultrathin skin
168   closing the pores.   The thickness of this layer is not fully homogeneous, being thinner where the
169   pores originally were. Membranes cast from solutions in DMF with higher polymer concentration
170   have a smoother morphology (Fig. S17), since the pores initially formed are also smaller, and less
171   chain reptation is required to form the dense layer. The membrane porosity and smoothness of the
172   formed dense layer depend on the casting solution viscosity, which is higher in NMP than in DMF
173   and increases as the polymer concentration increases (Fig. S18). Fig. 2G shows the nodular

174 morphology of the dense layer of a D325-2h membrane stained by ruthenium oxide, which reflects
175 a nanoporosity on a scale of 1 nm diameter or lower.
176   The crosssection SEM images (Fig. 2) reveal a highly porous structure below the ultrathin
177 dense layer, which is is retained even after the thermal treatment. Open interconnected pores are
178 also observed between larger cavities (Fig. 2c) facilitating the permeant transport. We assume that
179 the stability of the porous sublayer to collapse is favored by the high glass transition (T_g) in the
180 bulk of the polytriazole (above 350°C), due to preexistent π-π interactions which minimize the
181 rearrangement of the polymer chains during the crosslinking.
182

The stability of the crosslinked PTA-OH membranes and their morphology constituted by a ultrathin dense layer built on an asymmetric porous structure make them specially attractive for challenging applications in the chemical and petrochemical industry with a perspective of high selectivity aligned to low transport resistance. We first investigated the performance of the membranes for the filtration of solutions in polar (DMF) and apolar (toluene) solvents. This had the objective of confirming that the membrane integrity is maintained in a separation medium frequently used for chemical separations and gave us an overall evaluation of the membrane properties in terms of permeance and selectivity. The ultimate challenge for the membranes was testing them for crude oil fractionation. Fig. S19A shows how the permeance of different solvents varies with the inverse of their viscosity for D300-3h membranes. The linearity indicates that the transport follows Hagen-Poiseuille law and the separation is size-selective. Plots considering Hansen solubility parameters and molecular diameters (Fig. S19C-E), which have fitted well other nanofiltration systems (*18*) with a stronger solution-diffusion component for the transport, led to a poor correlation. No compaction was observed when testing with DMF, seen by a linear correlation of flux and pressure (Fig. S19E). The DMF permeance through D325-1h membranes remained constant in tests up to 70h (Fig. S20A) and practically recovered the starting permeance values when sequential tests in temperatures up to 90°C and back to 30°C (Fig. S20B) were performed. The rejection of methyl orange (MO) was high and stable (Fig. 20C). The permeances of membranes prepared from casting solutions in NMP and DMF under similar conditions were compared (Fig. S21). The MO size (molecular weight = 327 $g\,mol^{-1}$) is close to the membrane molecular weight cut-off (MWCO) measured at 30 and 65°C, with the rejection improving when the crosslinking temperature increases from 300 to 325°C (Fig. S21E, S21F). While the DMF permeance is higher for membranes prepared by casting from solutions in DMF and thermally treated for 1 to 2h, as the crosslinking reaction time increases, to 3h, the differences in performance practically disappear. When the filtration temperature was increased to 90°C, the MWCO of membranes N300-3h increased to 585 $g\,mol^{-1}$, the size of acid fuchsin. The increase of permeance of more than 2-fold by increasing the temperature from 30 to 90°C is due to a decrease of DMF viscosity (*19*) and also to some swelling of membranes crosslinked at milder conditions.

The DMF permeances of N300-3h membranes are at least 20 times higher than the values reported for state-of-the-art integrally asymmetric membranes at high temperature (*10, 20*) and comparable or even higher than those of the state-of-the-art thin-film composite membranes (Table S1) (*10, 12, 21-38*).

The membranes were then tested for the filtration of highly apolar systems like hydrocarbon solutions in toluene. The rejection of hexaphenylbenzene (Mw=534.7 $g\,mol^{-1}$) by N300-3h membranes is presented in Fig. S22A. Fig. 22B shows the separation of a mixture of three hydrocarbons, methylnaphthalene, 1,3-diisopropylbenzene, and pristane, dissolved in toluene, by a N325-1h. Similar rejection (60%) was obtained for the linear saturated hydrocarbon (268 $g\,mol^{-1}$) and the 1,3-diisopropylbenzene (162 $g\,mol^{-1}$), while methylnaphthalene (142.2 $g\,mol^{-1}$) was concentrated in the permeate side (Fig. 22B). The results indicate the potential of the polytriazole membranes to discriminate among different classes and sizes.

The main goal of this work is the development of membranes for the hydrocarbon fractionation. We then evaluated the performance of the membranes to fractionate dilute crude oil,

a feed closer to the real industrial feedstock. Based on the previous selectivity and permeance results, N300-1h, N300-3h and N325-1h membranes were selected for evaluating their performance in fractionating a 1:40 (volume ratio) solution of Arabian extra light crude oil (39 > API > 30 (American Petroleum Institute gravity)) in toluene. Atmospheric Pressure Photoionization Fourier Transform Ion Cyclotron Resonance Mass Spectrometry (FT-ICR MS) was used as the analytical method for the feed and permeate compositions. Fig. 3 and Fig. S23 show the separation results and the permeances connected to the experiments conducted at 30 and 65°C.

Fig. 3A-C shows the gray spectra of the diluted crude oil feed and the colored permeate spectra corresponding to the permeates of N300-1h, N300-3h, N325-1h, which are clear solutions (Fig. 3D). The spectra maxima corresponding to the fraction with highest abundance shifts from 400 to 350 and 300 g mol^{-1}, indicating that by choosing the right treatment conditions we can tune the properties of the selective layer and the separation. The N325-1h membrane leads to the enrichment of the lowest molecular weight fraction. The permeate has a higher ratio of components with a carbon number between 18 to 25, associated with kerosene fuel. The permeances during crude oil separation are in the range of 1.9 – 2.5 L m^{-2} h^{-1} bar^{-1} at 30°C, whereas at 65°C, the permeances increase almost 2 fold to 3.3 and 6 L m^{-2} h^{-1} bar^{-1} (Fig. 3F and S23D). The permeance values are 10 to 300-fold higher than recently reported systems, which show enrichment in the permeate of molecules with a molecular weight around 170 g mol^{-1} (*12*). In addition, when we permeated the crude oil mixture for 72h through the membrane, no significant decrease in permeance was observed (Fig. S23D).

We further evaluated the potential of N300-1h membranes for the fractionation of pure Arabian superlight crude oil (50 > API > 39) without prior dilution. The filtration experiments were carried out at 90 $^{\circ}$C to 150°C to decrease the oil viscosity and avoid pore blocking. GC-MS was used to analyze the components in the permeates. A standardized C$_7$-C$_{40}$ normal-saturated alkanes solution was utilized as reference to roughly correlate the GC retention times with the normal alkanes carbon numbers (Fig. 4 and Fig. S24). Fig. 4B shows the broad size distribution of the crude oil used as feed for the experiments leading to the permeates in Fig. 4A and 4C.

A highly effective enrichment of up to 80-95 % in hydrocarbons with carbon numbers lower than C$_{10}$ (molecular weight around 140 g mol^{-1}) was detected in the permeate (Fig. 4A), whereas the hydrocarbons between C$_{10}$-C$_{15}$ were in the range of 7 - 15%. Molecules with carbon numbers in the range of C$_{15}$-C$_{20}$ and higher than C$_{20}$ were only 4% and less than 1%, respectively.

A comprehensive two dimensional gas chromatography GCxGC data is shown in Fig. S25. These results complement the observations in Fig. 4 and S24, demonstrating that the membranes can discriminate between hydrocarbons of different sizes and discriminate between paraffins and aromatics as well. Low molecular weight hydrocarbons are of high potential usages as blending components for gasolines or lubricate base oils. By increasing the filtration temperature to 120 $^{\circ}$C, the polytriazole membrane led to a fraction 95 % enriched in smaller hydrocarbons (carbon numbers below C$_{15}$ corresponding to molecular weight around 180 g/mol), whereas the hydrocarbons between C$_{15}$-C$_{20}$ were only in the range of 3 - 4%. Fig. S25 indicates that paraffins and alkylbenzenes are the preferential compounds in the permeate at 90°C. Therefore, these data suggest that the polytriazole membranes could be integrated into a hybrid distillation system to fractionate crude oil.

270   The crude oil is a complex mixture. The effective separation of small molecules by the
271 membrane can be supported by a cluster formation between different components, which facilitates
272 only the permeation of small molecules and molecules that are not generating aggregates, like
273 linear hydrocarbons. Furthermore, the solvents – membrane interactions and different diffusion
274 and sorption mechanisms of each component in the crude oil can also contribute to the selection
275 between the paraffin/aromatics (*12*). The results obtained for hydrocarbons separation show that
276 moving from rather simple binary mixtures to dilute complex mixture, which has thousands of
277 different components, the advantages for the membrane could be preserved with a similar
278 molecular weight cutoff range.

279   In addition, the possibility of tuning the membranes separations properties by controlling
280 the crosslinking conditions opens new perspectives of fractionation procedures. For example,
281 using as feed a 1:1 mixture of Arabian superlight oil (39 > API > 30) to toluene (volume ratio)
282 instead of 1:40 to toluene, and a D300-1h membrane, which has a thin layer with looser structure
283 than the most crosslinked ones, it is possible to separate the larger molecules in the first stage, such
284 as asphaltene. This is demonstrated by the lighter color of the permeate and by the FT-ICR-MS
285 spectra (Fig. 4C) with lighter but still broad distribution of the masses. The permeate obtained in
286 the first stage was utilized as feed in the second stage using the more crosslinked D325-1h
287 membrane with a tighter layer. The GC chromatogram shows that more than 90% of the
288 hydrocarbons with carbon numbers below C10 were concentrated in the permeate side (Fig. 4D).

289   The results reported here show that by rationally selecting the polymer structure and
290 combining the classical NIPS method with thermally crosslinking, it is possible to obtain
291 promising membranes for a highly challenging chemical separation: the fractionation of crude oil.
292 The versatility of the polytriazole in terms of processability and crosslinking allows obtaining
293 polymeric membranes with a tailored selective layer using a method that is easy to scale up. The
294 tunable selectivity and permeances of the ultrathin polytriazole layer make these membranes
295 suitable to be integrated into a cascade system for a specific range of hydrocarbons separation.
296 High thermal stability permits testing a wide feed mixture in different conditions, suggesting that
297 the polytriazole membranes can be integrated into hybrid membrane configurations for energy-
298 efficient crude oil fractionation.

299

300

301

References and Notes

1. P. Marchetti, M. F. Jimenez Solomon, G. Szekely, A. G. Livingston, Molecular Separation with Organic Solvent Nanofiltration: A Critical Review. *Chem. Rev.* **114**, 10735-10806 (2014).

2. D. S. Sholl, R. P. Lively, Seven chemical separations to change the world. *Nature* **532**, 435-437 (2016).

3. R. P. Lively, D. S. Sholl, From water to organics in membrane separations. *Nat. Mater.* **16**, 276-279 (2017).

4. P. Vandezande, L. E. M. Gevers, I. F. J. Vankelecom, Solvent resistant nanofiltration: separating on a molecular level. *Chem. Soc. Rev.* **37**, 365-405 (2008).

5. H. B. Park, J. Kamcev, L. M. Robeson, M. Elimelech, B. D. Freeman, Maximizing the right stuff: The trade-off between membrane permeability and selectivity. *Science* **356**, eaab0530 (2017).

6. S. P. Nunes *et al.*, Thinking the future of membranes: Perspectives for advanced and new membrane materials and manufacturing processes. *J. Membr. Sci.* **598**, 117761 (2020).

7. W. J. Koros, C. Zhang, Materials for next-generation molecularly selective synthetic membranes. *Nature Materials* **16**, 289-297 (2017).

8. B. Van der Bruggen, in *Membrane Operations: Innovative Separations and Transformations*. (John Wiley & Sons, 2009), pp. 45-61.

9. K. Vanherck, G. Koeckelberghs, I. F. J. Vankelecom, Crosslinking polyimides for membrane applications: A review. *Progr. Polym. Sci.* **38**, 874-896 (2013).

10. J. D. Burgal, L. Peeva, A. Livingston, Negligible ageing in poly(ether-ether-ketone) membranes widens application range for solvent processing. *J. Membr. Sci.* **525**, 48-56 (2017).

11. M. Cook, P. R. J. Gaffney, L. G. Peeva, A. G. Livingston, Roll-to-roll dip coating of three different PIMs for Organic Solvent Nanofiltration. *J. Membr. Sci.* **558**, 52-63 (2018).

12. K. A. Thompson *et al.*, N-Aryl-linked spirocyclic polymers for membrane separations of complex hydrocarbon mixtures. *Science* **369**, 310-315 (2020).

13. J. F. Brennecke, B. Freeman, Reimagining petroleum refining. *Science* **369**, 254-255 (2020).

14. S. Chisca, G. Falca, V. E. Musteata, C. Boi, S. P. Nunes, Crosslinked polytriazole membranes for organophilic filtration. *J. Membr. Sci.* **528**, 264-272 (2017).

15. E. Jin *et al.*, Two-dimensional sp2 carbon–conjugated covalent organic frameworks. *Science* **357**, 673-676 (2017).

16. S. Chisca *et al.*, Organic solvent and thermal resistant polytriazole membranes with enhanced mechanical properties cast from solutions in non-toxic solvents. *J. Membr. Sci.* **597**, 117634 (2020).

17. M. Chowdhury, R. D. Priestley, Discrete mobility on the surface of glasses. *PNAS* **114**, 4854-4856 (2017).

18. S.-H. Park *et al.*, Hydrophobic thin film composite nanofiltration membranes derived solely from sustainable sources. *Green Chem.* **23**, 1175-1184 (2021).

19. J. M. Bernal-García, A. Guzmán-López, A. Cabrales-Torres, A. Estrada-Baltazar, G. A. Iglesias-Silva, Densities and viscosities of (N, N-dimethylformamide+ water) at atmospheric pressure from (283.15 to 353.15) K. *J. Chem. Eng. Data* **53**, 1024-1027 (2008).

20. J. H. Kim *et al.*, A compact and scalable fabrication method for robust thin film composite membranes. *Green Chem.* **20**, 1887-1898 (2018).

343   21.   S. Darvishmanesh, J. Degrève, B. Van der Bruggen, Mechanisms of solute rejection in solvent
344   resistant nanofiltration: the effect of solvent on solute rejection. *Phys. Chem. Chem.Phys.* **12**,
345   13333-13342 (2010).

346   22.   S. Darvishmanesh *et al.*, Performance of solvent resistant nanofiltration membranes for purification
347   of residual solvent in the pharmaceutical industry: experiments and simulation. *Green Chem.* **13**,
348   3476-3483 (2011).

349   23.   H. Siddique *et al.*, Membranes for organic solvent nanofiltration based on preassembled
350   nanoparticles. *Ind. & Eng. Chem. Res.* **52**, 1109-1121 (2013).

351   24.   H. Werhan, A. Farshori, P. R. von Rohr, Separation of lignin oxidation products by organic solvent
352   nanofiltration. *J. Membr. Sci.* **423**, 404-412 (2012).

353   25.   R. Othman, A. W. Mohammad, M. Ismail, J. Salimon, Application of polymeric solvent resistant
354   nanofiltration membranes for biodiesel production. *J. Membr. Sci.* **348**, 287-297 (2010).

355   26.   M. Morshed, H. Simonaire, H. Alem, D. Roizard, Investigation of OSN properties of PDMS
356   membrane for the retention of dilute solutes with potential industrial applications. *J. Appl. Polym.*
357   *Sci.* **137**, 48359 (2020).

358   27.   Z. F. Gao, G. M. Shi, Y. Cui, T.-S. Chung, Organic solvent nanofiltration (OSN) membranes made
359   from plasma grafting of polyethylene glycol on cross-linked polyimide ultrafiltration substrates. *J.*
360   *Membr. Sci.* **565**, 169-178 (2018).

361   28.   A. A. Tashvigh, L. Luo, T.-S. Chung, M. Weber, C. Maletzko, Performance enhancement in
362   organic   solvent   nanofiltration   by   double   crosslinking   technique   using   sulfonated
363   polyphenylsulfone (sPPSU) and polybenzimidazole (PBI). *J. Membr. Sci.* **551**, 204-213 (2018).

364   29.   M. F. Jimenez-Solomon, Q. L. Song, K. E. Jelfs, M. Munoz-Ibanez, A. G. Livingston, Polymer
365   nanofilms with enhanced microporosity by interfacial polymerization. *Nat. Mater.* **15**, 760-767
366   (2016).

367   30.   S. Karan, Z. Jiang, A. G. Livingston, Sub–10 nm polyamide nanofilms with ultrafast solvent
368   transport for molecular separation. *Science* **348**, 1347-1351 (2015).

369   31.   J. H. Kim *et al.*, A robust thin film composite membrane incorporating thermally rearranged
370   polymer support for organic solvent nanofiltration and pressure retarded osmosis. *J. Membr. Sci.*
371   **550**, 322-331 (2018).

372   32.   L. F. Villalobos, T. Huang, K. V. Peinemann, Cyclodextrin films with fast solvent transport and
373   shape-selective permeability. *Adv. Mater.* **29**, 1606641 (2017).

374   33.   J. Liu, D. Hua, Y. Zhang, S. Japip, T. S. Chung, Precise molecular sieving architectures with janus
375   pathways for both polar and nonpolar molecules. *Advanced Materials* **30**, 1705933 (2018).

376   34.   T. Huang, T. Puspasari, S. P. Nunes, K. V. Peinemann, Ultrathin 2D-layered cyclodextrin
377   membranes for high-performance organic solvent nanofiltration. *Adv. Funct. Mater.* **30**, 1906797
378   (2020).

379   35.   T. F. Huang *et al.*, Molecularly-porous ultrathin membranes for highly selective organic solvent
380   nanofiltration. *Nat. Comm.* **11**, 5882 (2020).

381   36.   M. Amirilargani *et al.*, Melamine-Based Microporous Organic Framework Thin Films on an
382   Alumina Membrane for High-Flux Organic Solvent Nanofiltration. *ChemSusChem* **13**, 136-140
383   (2020).

384   37.   C. Li *et al.*, Covalent organic frameworks (COFs)-incorporated thin film nanocomposite (TFN)
385   membranes for high-flux organic solvent nanofiltration (OSN). *J. Membr. Sci.* **572**, 520-531
386   (2019).

387   38.   J. Liu *et al.*, Self-standing and flexible covalent organic framework (COF) membranes for
388   molecular separation. *Sci. Adv.* **6**, eabb1110 (2020).

389

390

Author contributions:

Conceptualization: SC, SN

Methodology and investigation: SC (design, membrane preparation, SEM, separation performance), VM (mechanical properties, TEM, DSC), GF (separation performance), WZ (FT-ICR MS and GC-MS), EAH (NMR), AHE (EPR), MA (TGA-MS)

Funding acquisition and supervision: SN

Writing – original draft: SC, SN

Writing – review & editing: SC, SN

Competing interests: The authors declare no competing interests. SC, VM, and SN are inventors on a patent application US 63/174,376 recently submitted by KAUST.

Data and materials availability: All data are available in the manuscript or the supplementary material.

Supplementary Materials

Materials and Methods

Figs. S1 to S25

Table 1

Fig. 1. Structure and characterization of thermally crosslinking membranes. (**A**) Structure of PTA-OH and the proposed crosslinked network. (**B**) 2D ^{1}H-^{13}C heteronuclear correlation (HETCOR) and ^{13}C-^{13}C (with proton driven spin-diffusion (PDSD)) NMR spectra of the pristine PTA-OH (blue) and of the membrane treated at 325°C for 2h (red). The peaks indicated by letters are assigned to the carbon atoms in the structures depicted in (A). (**C**) ^{17}O PRESTO-QCPMG DNP spectra of pristine (blue) and treated samples (red). (**D**) ^{1}H-^{15}N CP-MAS HETCOR spectra of pristine (blue) and treated samples (red).

Fig. 2. Morphology of membranes cast from 16 wt% PTA-OH solutions in DMF. (**A-C**) Cross-sectional SEM images of membranes treated at 300°C for 3h (D300-3h). (**D-G**) TEM cross-sectional images (D) Untreated PTA-OH membrane. (E) D325-1h membrane (inset: higher magnification of the selective layer). (F and G) Selective layer of a D325-2h membrane.

Fig. 3. Polytriazole membrane performance with dilute crude oil as feed. (**A-C**) FT-ICR MS spectra of the feed and permeate in experiments conducted at 30°C with 1:40 (volume ratio)

430 Arabian super light crude oil to toluene mixtures, using thermally treated membranes cast from
431 16% PTA-OH solutions in NMP (N300-1h, N300-3h and N325-1h). (**D**) Photographs of permeate,
432 feed, and retentate after filtrations at 65°C. (**E**) Double bond equivalent vs. carbon number for the
433 feed and the permeate using a N325-1h membrane. (**F**) Permeance of dilute crude oil solutions at
434 30 °C and 65 °C using a N300-3h membrane.

435 **Fig. 4**. **Crude-oil separation by polytriazole membranes**(**A**) Gas chromatograms of crude oil
436 fractions in different temperatures: 90°C, 120°C, and 150°C. The inset photograph shows the
437 permeate obtained at 90°C. (**B**) FT-ICR MS spectra of the Arabian superlight crude oil. Inset
438 photograph of the crude oil feed. (**C**) FT-ICR MS spectra of the retentate and permeate in
439 experiments conducted at 30°C with 1:1 (volume ratio) Arabian extra light crude oil to toluene
440 mixtures, using a D300-1h membrane. The inset photograph of the retentate and permeate. (**D**)
441 Gas chromatograms of the permeate obtained at 90°C using a D325-1h membrane and as feed the
442 permeate depicted in (C). Inset photograph of the feed permeate and retentate.

443

444

445 Fig. 1
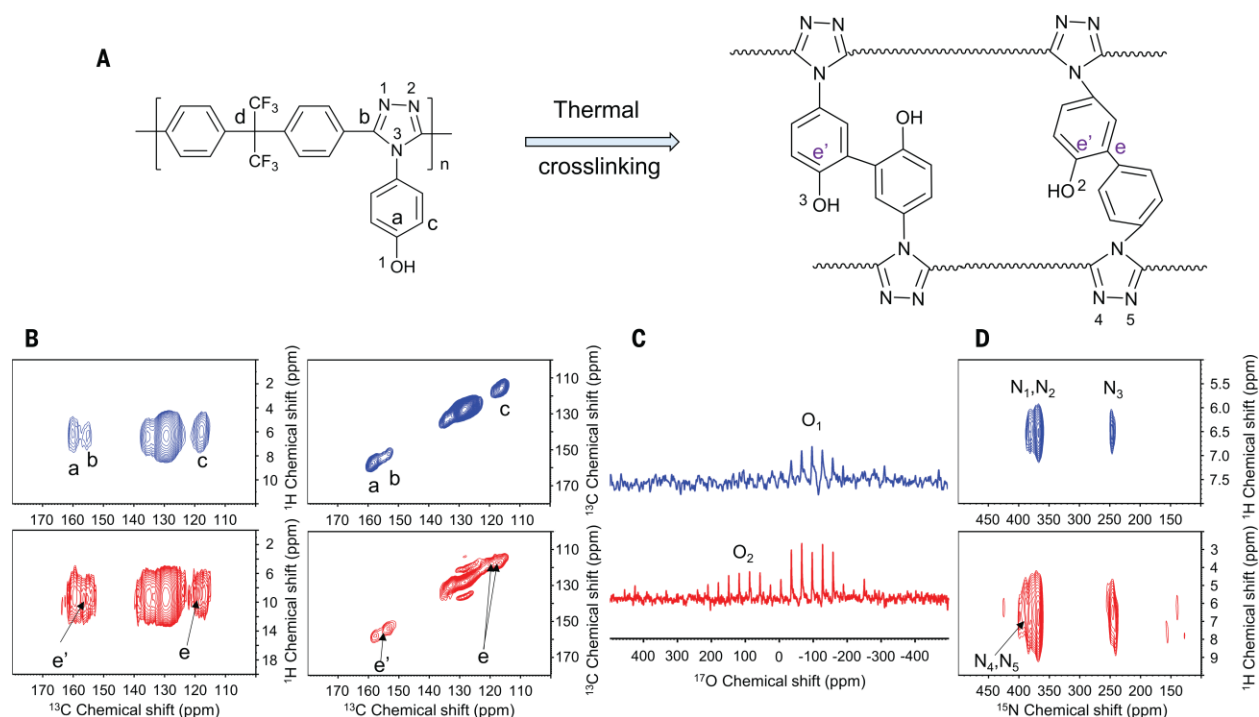
446

447

448 Fig. 2
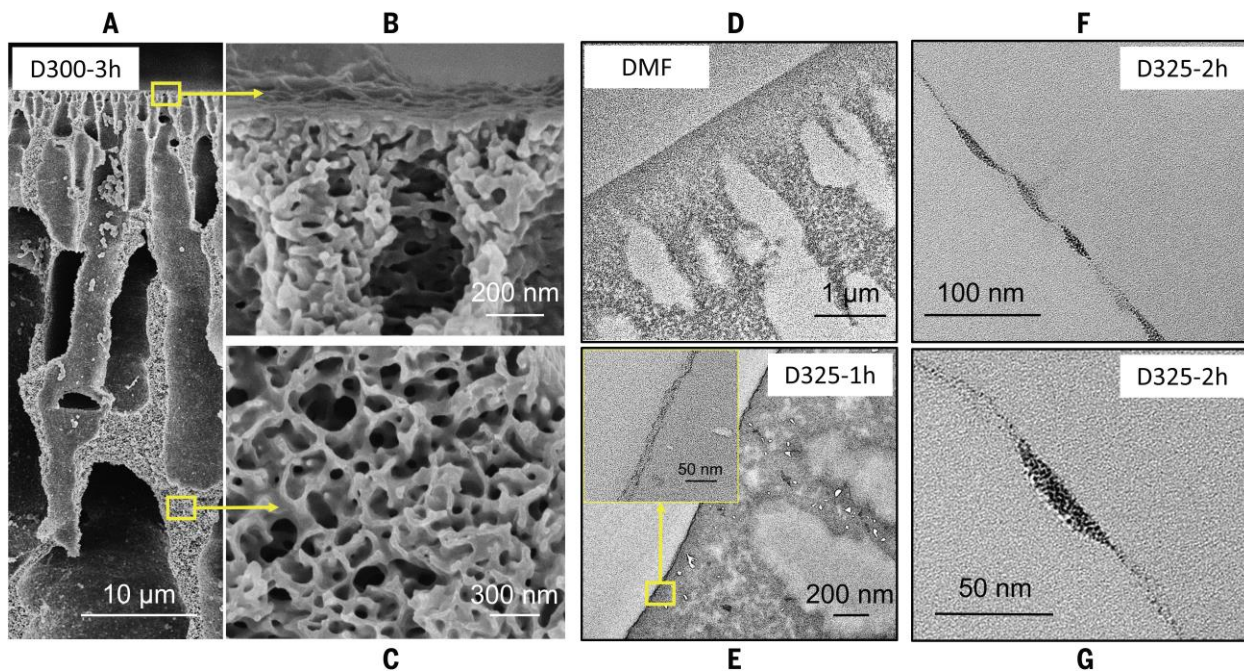
449
450

451   Fig. 3

452
453
454
455
456

14

457   Fig. 4

458

459

Science

∧AAAS
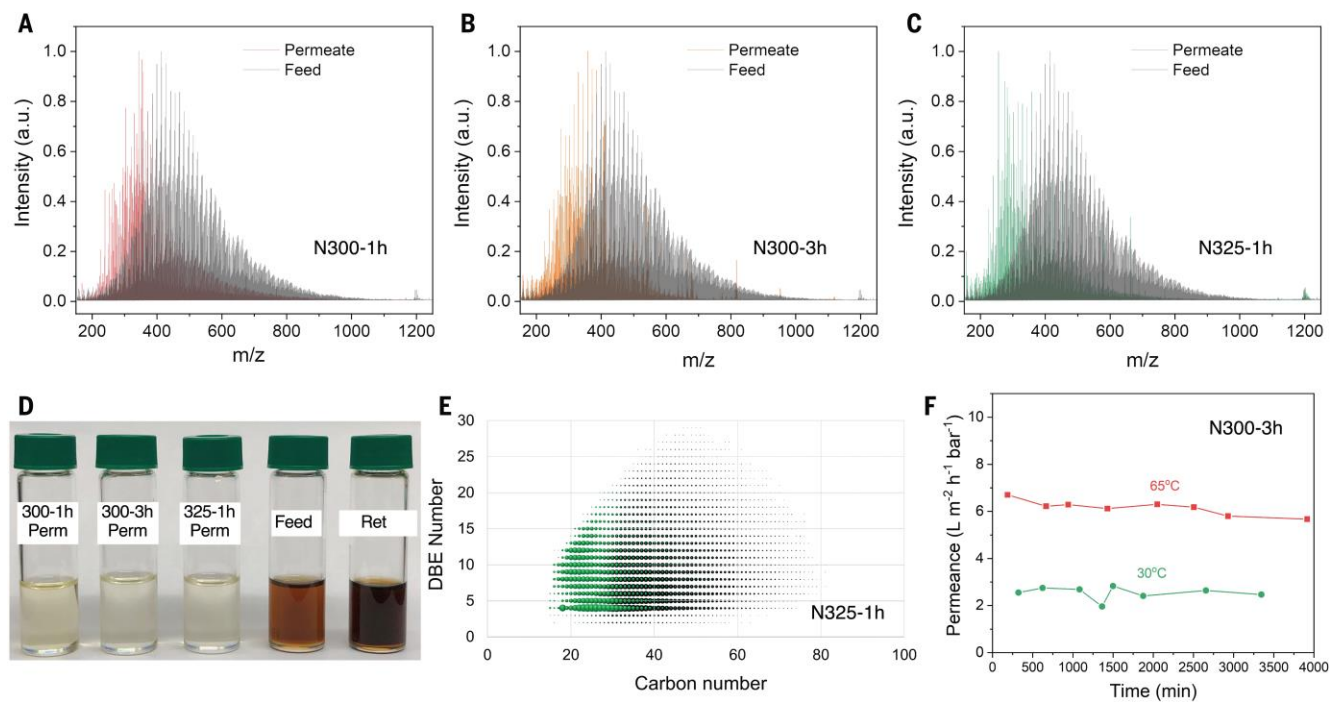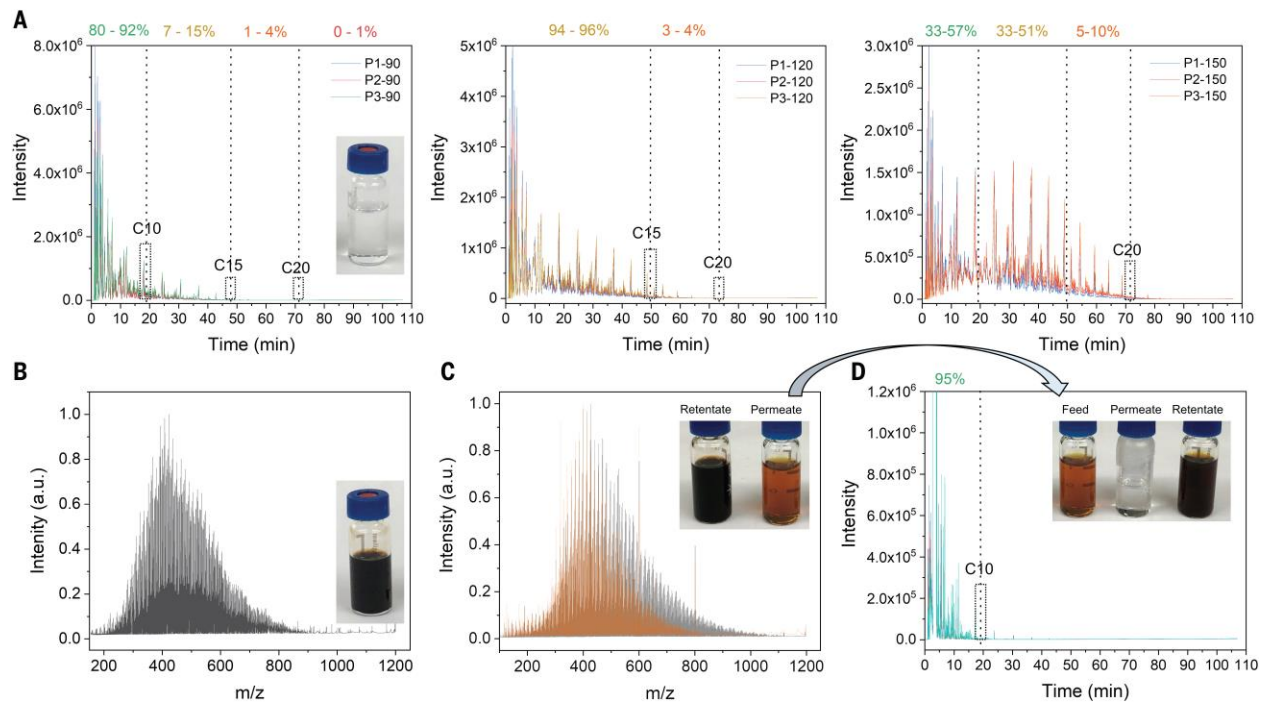
Supplementary Materials for

Polytriazole membranes with ultrathin tunable selective layer for crude oil fractionation

Stefan Chisca[1,2], Valentina-Elena Musteata[1,3], Wen Zhang[3†], Serhii Vasylevskyi[3], Gheorghe Falca[1,2], Edy Abou-Hamad[3], Abdul-Hamid Emwas[3], Mustafa Altunkaya[3], Suzana P. Nunes[1,2,4,5*]

[1]Environmental Science and Engineering Program, Biological and Environmental Science and Engineering Division (BESE), King Abdullah University of Science and Technology (KAUST), , Thuwal, Saudi Arabia

[2]Advanced Membranes and Porous Materials (AMPM) Center, King Abdullah University of Science and Technology (KAUST)

[3]Core Labs, King Abdullah University of Science and Technology (KAUST),

[4]Chemical Science Program, Physical Science and Engineering Division (BESE), King Abdullah University of Science and Technology (KAUST)
[5]Chemical Engineering Program, Physical Science and Engineering Division (BESE), King Abdullah University of Science and Technology (KAUST)

Correspondence to: suzana.nunes@kaust.edu.sa

†Present address: Dept. Environmental Science, Stockholm University, 106 91 Stockholm, Sweden

This PDF file includes:

Materials and Methods

Figs. S1-S25

Table S1

1. Materials and Methods

Materials

Polyphosphoric acid 84% (PPA) and 4,4′-(hexafluoroisopropylidene) bis(benzoic acid) were purchased from Alfa Aesar, hydrazinium sulfate from VWR chemicals, 4-aminophenol, aniline, N-methyl-2-pyrrolidone (NMP), N,N′-dimethylformamide (DMF) (99.8%), C7-C40 saturated alkanes standard and all the other reagents were obtained from Sigma-Aldrich.

Methods

<u>Polymer synthesis</u>

The polytriazoles with hydroxyl groups (PTA-OH) and without (PTA) were synthesized in the lab by a two steps polycondensation reaction. The first step consists of the synthesis of a polyoxadiazole (POD) precursor, adapting a procedure reported before. First, 650 g of PPA and 60 g of 4,4′-(hexafluoroisopropylidene) bis(benzoic acid) were mixed in a 2000 mL three necks flask. The mixture was stirred at 90 °C under nitrogen until a homogeneous solution was formed, then 24 g of hydrazinium sulfate was added. The mixture was heated at 167 °C for 2-2.5 hours. The resulting highly viscous POD solution was precipitated in water and neutralized with 1 M NaOH. 55 g POD were then dissolved in 365 mL NMP at 90 °C under nitrogen in a 2000 mL three necks flask. When a homogeneous solution was obtained, approx. 2.2 g of PPA and 40 g of 4-aminophenol were added, and reaction mixture was heated to 195 °C for 72 h. The resulting brown-colored solution was precipitated in a large amount of distilled water and washed several times with hot water and methanol to remove the unreacted 4-aminophenol. A similar procedure was used to prepare polytriazole without OH groups, but instead of 4-aminophenol, aniline was used. The polymers were purified by re-precipitation from NMP three times. The PTA-OH synthesized and used in this work was 98% functionalized, as confirmed by NMR characterization.

522 Membrane preparation

523   The polytriazole membranes were prepared by non-solvent-induced phase separation

524 (NIPS). 16 wt% polytriazole solutions in N-methyl-2-pyrrolidone (NMP) or N,N′-

525 dimethylformamide (DMF) were cast on a glass plate using a doctor blade with 200 μm gap. The

526 polymer membranes were obtained by immersing the glass plate into a distillate water bath. The

527 membranes were washed with distillate water for 72 h to eliminate any remaining solvent and

528 freeze-dried. To crosslinkthe polytriazole membranes by thermal treatment, we used a

529 Lindberg/Blue M™ 1200°C Split-Hinge Tube Furnaces. The furnace heating rate was set

530 at 5°C per minute. The obtained integral asymmetric membranes were thermally treated in the

531 furnace under an air atmosphere at 120°C for 30 min before continuing the treatment to 300°C for

532 1h, 2h, and 3h, and to 325°C for 1h and 2h.

533   The PTA-OH membranes are referred to as N- or D- depending on the solvent used for

534 casting. The temperature and time of thermal treatment are then indicated. For example, D-300-2h

535 is a membrane cast from solutions in DMF, submitted to thermal treatment at 300°C for 2h.

536

537 Molecular weight characterization

538   Gel permeation chromatography (GPC) was used to analyze the molecular weight of the

539 synthesized polytriazole. The GPC system was equipped with an Agilent refractive index detector,

540 and DMF was used as a mobile phase at 45°C. Molecular weight was determined from a calibration

541 curve obtained using polystyrene standards.

542 Spectroscopic characterization

543   The chemical changes during thermal treatment were evaluated by spectroscopic methods.

544

545   *Fourier Transform Infrared (FTIR) spectroscopy* was performed on a Nicolet 6700 FT-IR

546 System. 16 scans with a spectral resolution of 4 cm^{-1} were recorded for each FTIR spectrum.

547

548   *Electron Paramagnetic Resonance (EPR)*

549   Continuous-wave Bruker EMX PLUS spectrometer operation at x-band (BrukerBioSpin,

550 Rheinstetten, Germany) was used to record all EPR spectra at room temperature. The spectrometer

551 is equipped with standard high Q resonator ER4122SHQE for high sensitivity CW-EPR and

operating at (9.384688) GHz. All spectra were recorded under the same conditions by collecting 5 scans with 25 dB microwave attenuation with 5 G modulation amplitude and 100 kHz modulation frequency. Bruker Xenon software (Bruker BioSpin, Rheinstetten, Germany) was used for data collection, and origin software was used for plotting the spectra.

Solid-State Nuclear Magnetic Resonance (NMR) Spectroscopy

One-dimensional ^{1}H MAS and ^{13}C CP/MAS solid-state NMR spectra were recorded on Bruker AVANCE III spectrometers operating at 400 or 600 MHz resonance frequencies for ^{1}H. Experiments at 400 MHz employed a conventional double-resonance 4 mm CP/MAS probe, while experiments at 600 MHz utilized a 2.5 mm double-resonance probe. Dry nitrogen gas was utilized for sample spinning to prevent degradation of the samples. NMR chemical shifts are reported with respect to the external references TMS and adamantane. For ^{13}C CP/MAS NMR experiments, the following sequence was used: 90° pulse on the proton (pulse length 2.4 s), then a cross-polarization step with a contact time of typically 2 ms, and finally, the acquisition of the ^{13}C signal under high-power proton decoupling. The delay between the scans was set to 5 s to allow the complete relaxation of the ^{1}H nuclei, and the number of scans ranged between 10000 and 20000 for ^{13}C and was 32 for ^{1}H. An exponential apodization function corresponding to a line broadening of 80 Hz was applied prior to Fourier transformation.

Two-dimensional ^{1}H-^{1}H double-quantum (DQ) experiments were recorded on a Bruker AVANCE III spectrometer operating at 600 MHz with a conventional double resonance 3.2 mm CP/MAS probe, according to the following general scheme: excitation of DQ coherences, t_1 evolution, z-filter, and detection. The spectra were recorded in a rotor synchronized fashion in t_1 by setting the t_1 increment equal to one rotor period (45.45 μs). One cycle of the standard back-to-back (BABA) recoupling sequences was used for the excitation and reconversion period. Quadrature detection in w_1 was achieved using the States-TPPI method. A MAS frequency of 22 kHz was used. The 90° proton pulse length was 2.5 μs, while a recycle delay of 5 s was used. A total of 128 t_1 increments with 128 scans per each increment were recorded. The DQ frequency in the w_1 dimension corresponds to the sum of two single quantum (SQ) frequencies of the two coupled protons and correlates in the w_2 dimension with the two corresponding proton resonances.

582   2D $^1H-^{13}C$ heteronuclear correlation (HETCOR) solid-state NMR spectroscopy

583   experiments were conducted on a Bruker AVANCE III spectrometer using a 2.5 mm MAS probe.

584   The experiments were performed according to the following scheme: 90° proton pulse, t_1 evolution

585   period, CP to ^{13}C, and detection of the ^{13}C magnetization under TPPM decoupling. For the cross-

586   polarization step, a ramped radio frequency (RF) field centered at 75 kHz was applied to the

587   protons, while the ^{13}C channel RF field was matched to obtain an optimal signal. A total of 64 t_1

588   increments with 2000 scans each were collected. The sample spinning frequency was 15 kHz.

589   Using a short contact time (0.2 ms) for the CP step, the polarization transfer in the dipolar

590   correlation experiment was verified to be selective for the first coordination sphere to lead to

591   correlations only between pairs of attached $^1H-^{13}C$ spins (C−H directly bonded).

592   2D ^{13}C-^{13}C spectra were recorded using a 2 s recycle delay, 10 ms (F2) and 1.3 ms (F1)

593   acquisition time, and an accumulation of 256 scans (both CP and DE). ^{13}C-^{13}C mixing was

594   achieved through proton-driven spin-diffusion (PDSD) using phase-alternated-recoupling-

595   irradiation-schemes (PARIS) for 120 ms (CP) or 200 ms (DE) mixing. 70 kHz SPINAL64 1H

596   decoupling was applied during both direct and indirect dimensions.

597

598   *Dynamic Nuclear Polarization NMR spectroscopy (DNP).*

599   For the DNP experiments, samples were prepared by incipient wetness impregnation of

600   polymeric membranes with radical TEKPol solutions. The solutions consisted of 16 mM TEKPol

601   (TEKPol, MW= 905 g/mol) in 1,1,2,2-tetrachloroethane (TCE). TEKPol was dried under a high

602   vacuum (10-4 mbar), and the solvent was stirred over calcium hydride and then distilled in the

603   vacuum. The compound was finely ground in a mortar and pestle prior to the preparation of DNP

604   experiments. In a typical experiment, 15 mg of the polymeric samples were impregnated with the

605   appropriate volume of 16 mM solution of TEKPol (nTEKPol = 0.5 - 1.2 μmol/sample) and packed

606   into a 3.2 mm o.d. sapphire rotor capped with a Teflon plug. The packed samples were immediately

607   inserted into the pre-cooled DNP probe for experiments.

608   The data were acquired on a 263 GHz/400 MHz Avance III Bruker DNP solid-state NMR

609   spectrometer equipped with a 3.2 mm Bruker triple resonance low temperature magic angle

610   spinning (LTMAS) probe and the experiments were performed at ca. 100 K with a 263 GHz

611   gyrotron. The sweep coil of the main magnetic field was set for the microwave irradiation

612   occurring at the 1H positive enhancement maximum of the TEKPol biradical. For the ^{15}N CP-

MAS DNP experiments, the acquisition parameters included a 3 s repetition delay and a 1H π/2 pulse length of 2.3 µs to afford 100 kHz 1H decoupling using the SPINAL 64 method. The contact time was typically 4 ms for the cross-polarization experiments. The MAS frequency varied between 8 and 12 kHz. The 2D ^{1}H–^{15}N HETCOR spectra were acquired with 2048 scans per t1 increment, 96 individual increments, and a contact time of 4 ms. DUMBO-1 homonuclear 1H decoupling was applied, and the proton chemical shifts were corrected by applying a scaling factor of 0.57.

^{17}O PRESTO-QCPMG experiments were performed under MAS at 10 kHz with 160 µs (2 rotor periods) of dipolar recoupling. The ^{17}O central-transition selective 90 and 180° pulses lasted 5 and 10 µs, respectively. The spikelet separation was set to 1.25 kHz, and 40k scans were acquired with a 4 s recycle delay.

The ^{17}O{1H} PRESTO-QCPMG HETCOR experiments were acquired using the same conditions as the 1D spectra with 3000 scans per t1 increment. Frequency-switched Lee−Goldberg homonuclear decoupling was applied during t1 to improve the resolution in the ^{1}H dimension, and the States-TPPI method was used for phase-sensitive detection.

Thermal, morphological, and mechanical characterization

The thermogravimetric analysis (TGA) was performed on a TGA Q50, TA Instrument, under air atmosphere from 25 to 800 °C, with a heating rate of 10 °C min^{-1}. The analysis of evolved gases during the membrane crosslinking was conducted for selected samples on a thermal analyzer (STA, NETZSCH STA TG/DSC 449 F1 Jupiter®) coupled with a mass spectrometer. The samples were in this case heated in a nitrogen atmosphere with a flow rate of 70 mL/min. The sample was placed in a standard alumina crucible. For the analysis of the evolved gases, a NETZSCH Aeolos® QMS 403 mass spectrometer was connected via a heated capillary to the heated adapter head of the thermal analyzer outlet. The temperature of the connections and the MS inlet was set to 250°C. The sample was measured in the temperature range from 25 to 325°C at a heating rate of 5 °C /min and kept isothermally for 1 h.

The glass transition temperature (T_g) of the hydroxy-polytriazole was measured by differential scanning calorimetry (DSC) on a TA DSC250 instrument, with a heating rate of 10°C min^{-1}.

644   The morphology of pristine and thermally treated membranes were investigated by
645 Scanning Electron Microscopy (SEM) on a Nova Nano microscope, using a 3-5 kV voltage and a
646 working distance of 3-5 mm. The morphology was also studied by Transmission Electron
647 Microscopy (TEM). Initially, the films were embedded in epoxy resin at 60 °C, and then ultrathin
648 sections (70 nm) were cut using an ultramicrotome (Leica EM UC6). The membranes were imaged
649 on a Titan CT (FEI company) microscope operating at 300 kV after they were stained with
650 ruthenium oxide.

651   The membrane mechanical characterization was performed on a TA Instruments Q850
652 Dynamic Mechanical Analyzer in tensile mode. Rectangular samples (15x5 mm) were cut from
653 the membranes with 70–80 μm thickness. The stress-strain curves were recorded using a force
654 ramp of 0.1 N/m, at 25 °C. Five samples were tested for each membrane. The ultimate tensile
655 properties are calculated as the average of stress and strain at break. A strain–recovery analysis
656 was performed by subjecting membranes to a stress of 1 MPa for 20 min, followed by a recovery
657 period of 80 min with removed stress. The applied stress level was chosen to ensure that the creep
658 measurements remained in the linear viscoelastic deformation regime of the stress-strain curve,
659 and it is comparable to the 5 bar pressure used for flux measurements. A small preload force of
660 0.01 N was applied to keep the sample right in the recovery regime.

661   The crystallinity and the d-spacing of the membranes were investigated using a Bruker D8
662 Advance diffractometer with Cu-Kα radiation source at 40 kV and 40 mV. The diffraction data
663 were measured in the range of 5°–60°.

664

665 <u>Membrane performance</u>

666

667   The membranes performances were investigating in a dead-end cell, using a membrane
668 area of 0.95 cm^2 and at pressures between 2 to 5 bar. The water permeance measurements of the
669 membranes prepared in DMF and NMP were performed at room temperature. The solvent
670 permeance was evaluated using equation 1:

671
$$J = \frac{Q}{A\Delta P} \tag{1}$$

672 where Q is the permeation rate (L h^{-1}), A is the active filtration area (m^2), and ΔP is the pressure
673 (bar).

674   The performances in various polar and non-polar organic solvents were evaluated at room

675   temperature using 3 different membranes. The solvents were tested consecutively following the

676   sequence: methanol, ethanol, acetone, hexane, heptane, toluene, and tetrahydrofuran.

677   The thermal treated membranes performances in DMF were consecutively measured at

678   different temperatures, from 30 to 90°C, using an active membrane area of 0.95 cm^{-2} at pressures

679   of 2-5 bar. Before the measurements, the membranes were immersed in DMF for 30 minutes and

680   then transferred in water before being mounted in the filtration cell. The membranes performances

681   were reported as an average of 3 different measurements. The long-time stability in DMF was

682   performed by direct heating the dead-end cell at 65°C. The permeances were measured for

683   approximately 67 h. The DMF flux at 30 and 65°C as a function of pressure was measured by

684   consecutively increase the pressure from 2 to 10 bar. For each pressure, the flux was measured for

685   at least 2h.

686   The rejection in DMF was investigated by filtrating methyl orange (MO, Mw=327 g mol^{-1}

687   ) and acid fuchsin (AF, Mw=585 g mol^{-1}). The concentration of the dyes in DMF was between 10

688   to 50 ppm. The rejection experiments were performed between 2 h and 4 h, discarding at least 10

689   mL before collecting the samples for analysis. The rejection (R) was evaluated using equation 2:

690

$$R(\%) = \left(1 - \frac{C_p}{C_f}\right) \times 100 \qquad\qquad (2)$$

691   where Cp is the solute concentration in the permeates, and C_f is the solute concentrations in the

692   feed. UV spectrometer (NanoDrop 2000c) was used to evaluate the separation of the dye

693   molecules.

694   The hydrocarbon rejection using binary mixture was investigated by dissolving

695   hexaphenylbenzene (Mw=534.7 g mol^{-1}) in toluene at a concentration of 100 ppm. UV

696   spectrometer (NanoDrop 2000c) and equation 2 were used to evaluate the separation. The filtration

697   was performed under 5 bar for 20h. For measuring multi-components rejection,

698   methylnaphthalene, 1,3-diisopropylbenzene, and pristane were dissolved in toluene in a ratio of 1

699   / 99 mol % of hydrocarbons/toluene. Gas chromatography was used to test the separation

700   performance. The filtration was performed under 5 bar for 48h. The binary and multicomponent

701   mixture experiments were carried out at 30°C. The fractionation of dilute crude oil was

702   investigated by consecutively heating at 30 and 65°C. The Arabian extra light crude oil was diluted

703   in toluene in a volume ratio of 1:40. To measure the permeance during the experiments, we

704   collected samples at different intervals (4h to 10h). The initial feed volume was 200 mL, and the

705   total volume permeated was between 20 to 80 mL. The permeation experiment (consecutively

706   permeating at 30 and 65°C) was carried out for approximately 100 h. The feed and the permeances

707   were analyzed using FT-ICR MS. The filtration experiments with pure Arabian super light crude

708   oil were performed by consecutively heating at 90, 120, and 150°C under 15 bar. The area of the

709   membranes for this experiment was between 0.95 and 3.14 cm^{-2}. Different fractions were collected

710   every 24 or 48h. The initial feed volume was 50 or 100 mL, and the total volume permeated was

711   between 10 to 17 mL. The permeation experiment (consecutively permeating at 90, 120, and

712   150°C) was carried out for approximately 10 days. This experiment was confirmed using 3

713   different membranes. For the experiments with crude oil (dilute Arabian extra light crude crude

714   oil and pure Arabian super light crude oil), vials with rubber septum were connected to the

715   permeate side tube to diminish the evaporation of the lighter components from the permeance. The

716   building pressure within the vials was equalized by the aid of a needle. The permeates obtained

717   using pure Arabian super light crude oil as feed were investigated using the GC. To identify the

718   components in the permeates a standardized C_7-C_{40} saturated alkanes solution in hexane was used.

719   The enrichment of the hydrocarbons in the permeance was calculated by integrating the GS peaks

720   below C_{10}, in the range of C_{10}-C_{15} and C_{15}-C_{20}, and higher than C_{20}. The crude oil fractionation

721   experiment was performed starting with a 1:1 feed mixture of Arabian extra light toluene. For this

722   experiment, we used membranes with 0.95 cm^{-2}. The initial feed mixture was 70 mL, and in the

723   first stage, we collected 36 mL. For the second step, the collected amount in the first step was

724   utilized as feed, and we permeated 10 mL out of this.

725   The gas chromatography-mass spectrometry (GC MS) was performed on an Agilent 7890A

726   GC with both flame ionization detector (FID) and quadrupole mass spectrometer (Agilent 5975C

727   MSD) via a three-way splitter. 2μL of the permeated oil sample was injected into the split/splitless

728   inlet under 300 °C. The split ratio of 10:1 was employed. The sample was further separated on a

729   HP-5MS column (30 m x 250 μm x 0.25 μm with Agilent part number 19091S-433) with the flow

730   rate of 3 mL/min. The oven was kept at 40°C for 1 minute and increased to 250°C with a rate of

731   2°C/min. The elutes were separated into 2 flows, for FID and MSD separately, after the column

732   separation. The MSD peaks were used for structural elucidation, and FID signals were used for

733   quantitative analysis. The GC was calibrated with C7-C40 n-alkanes. The calculation of carbon

734   number distribution is roughly based on the retention times of individual normal alkane standards.

735   The oils were further characterized on a Bruker SolariX XR 9.4 Tesla Fourier-transform

736   ion cyclotron resonance mass spectrometer (FT ICR MS, BRUKER DALTONIK GmbH, Bremen,

737   Germany) with an atmospheric pressure photoionization ionization (APPI) source. The instrument

738   was first calibrated with low molecular weight polystyrene beforehand. The samples were diluted

739   in toluene and directly infused into the ionization sources by a syringe pump with a flow rate of

740   10 uL/min. The APPI source was operated with a nebulizer pressure of 2.5bar, vaporizer

741   temperature of 400 °C, dry gas flow of 4.0L/min, and dry temperature of 220 °C. Each data set

742   was acquired with 8 Megawords sizes by accumulating 300 scans in the mass range of 150-1200

743   Da). The FT ICR MS spectra were further treated by the Bruker DataAnalysis V4.5 software; only

744   the peaks with S/N higher than 5 were considered for following chemical formula assignment. The

745   chemical formula assignment was performed with Composer software (Sierra Analytics, Modesto,

746   CA, USA). Giving an error range of ±0.5ppm, the most probable elemental composition of each

747   monoisotopic mass peak was calculated according to the determined accurate mass within the

748   chemical formula range of $C_{1-100}H_{1-200}N_{0-3}O_{0-3}S_{0-3}$. The resulting chemical formulas were further

749   sorted into different compound classes, such as radical hydrocarbon ions (HC), protonated

750   hydrocarbon ions (HC [H]), radical ions of hydrocarbons with one S atom (S), and so forth. Then,

751   the iso-abundance plot was used to display the distribution of certain compound classes in terms

752   of carbon number, double bond equivalent number, and abundance.

753   The GC×GC-TOF/MS analysis was performed using an Agilent 7890B gas chromatography

754   system (Agilent Technologies, Wilmington, Delaware), equipped with a Zoex ZX1 cryogenic

755   thermal modulator (Zoex Corporation, Houston, Texas) and a Jeol TOF MS (AccuTOF GCx-plus,

756   JEOL, Japan). The GC×GC system was consisted of a normal (non-polar x mid-polar) two-

757   dimensional column configuration. The first-dimension column was a 30 m nonpolar HP-5MS UI

758   capillary column (5%-Phenyl-methylpolysiloxane) with an internal diameter of 0.25 mm and a

759   stationary-phase film thickness of 0.25 μm. The second-dimension was a 1m mid polar BPX-50

760   capillary column (50% Phenyl Polysilphenylene-siloxane) with an internal diameter of 0.1 mm

761   and a film thickness of 0.1 μm. Helium (99.999%) was used as the carrier gas with a constant flow

762   rate of 0.8 mL min^{-1}. The GC × GC-TOF/MS injector temperature was maintained at 300 °C with

763   a split ratio of 150:1. The oven temperature was initially maintained at 80 °C for 1 min, and then

764 ramped to 325 °C at a rate of 2 °C min^{-1}. The modulation period was 6 s with pulse time 0.350 ms.

765 The mass spectrometer was operated in electron ionization (EI+) mode at 70 eV. The transfer line

766 and ion source temperatures were kept constant at 250 °C. The detector voltage of TOF was 2500

767 Volts and data were acquired at a rate of 50 Hz. Mass spectra were obtained from m/z 50 to 450.

768 The 2D data were processed and displayed using the GC ImageTM VersionTM 2.9 software

769 (Lincoln NE, USA). The NIST/EPA/NIH EI Mass Spectral Library 2.3 version was used to

770 confirm the identification.
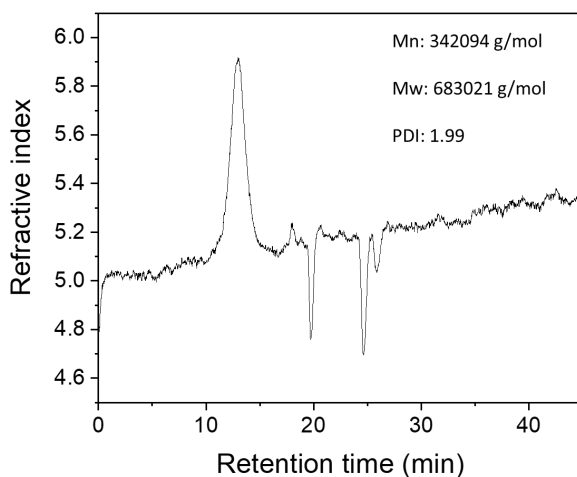
Fig. S1. GPC analysis of PTA-OH.

775
776
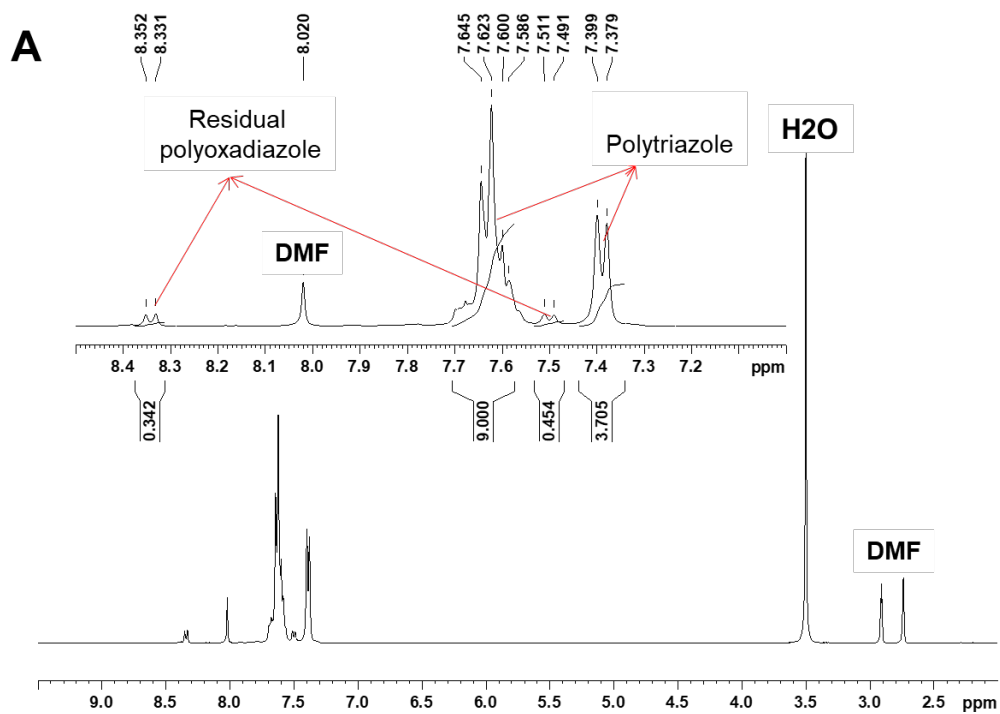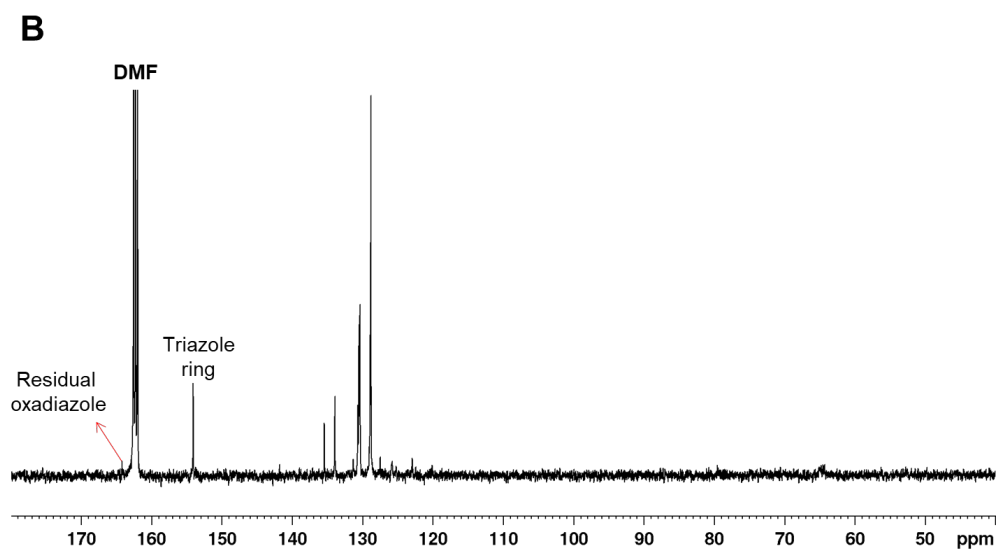
Fig. S2. NMR characterization of non-functionalized PTA in solution. (A) ^{1}H NMR and (B) ^{13}C NMR.

777
778
779
780
781
782
783

784

785

786
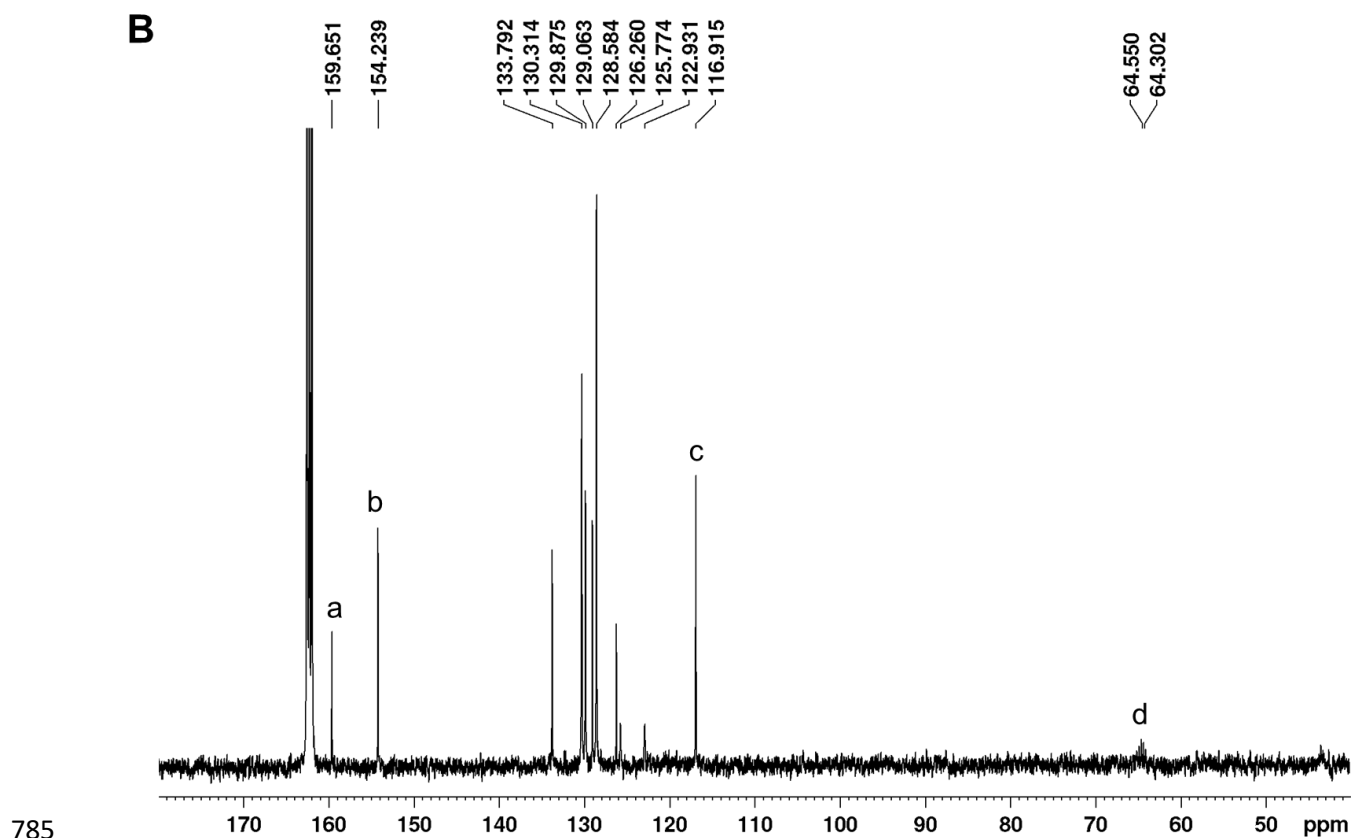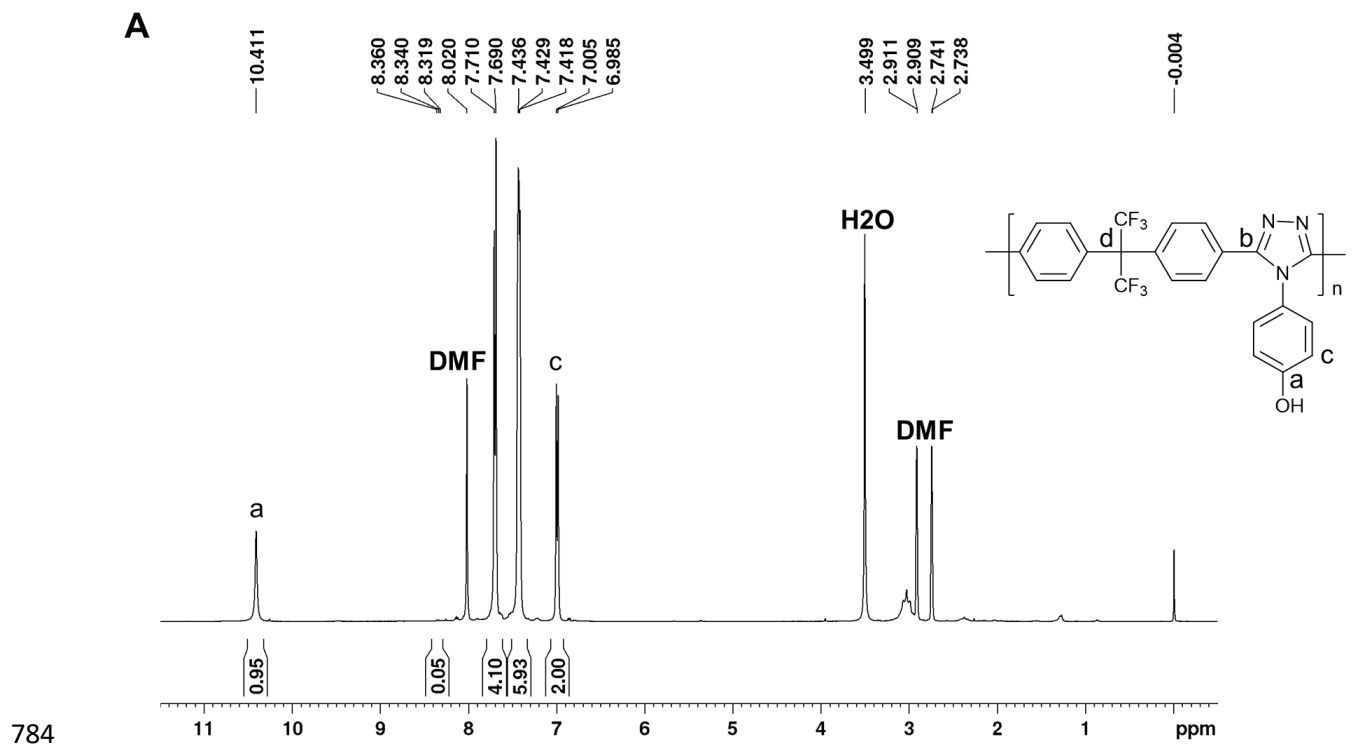
Fig. S3. NMR characterization of PTA-OH in solution. (A) ^{1}H NMR and (B) ^{13}C NMR.

787

788

Stability

DMF   HCl   H₂SO₄   NaOH   Piranha
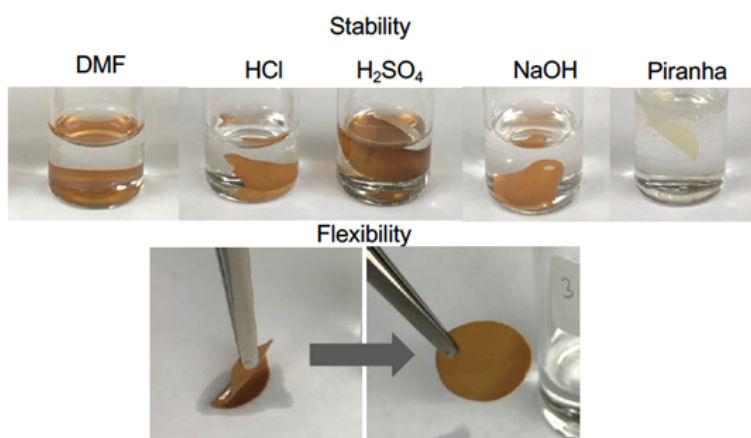
Flexibility

789
790
791 **Fig. S4.** Solvent stability test. Photographs of thermally treated PTA-OH immersed in DMF, acids,

792 and base conditions for more than 3 months. Demonstration of the flexibility of the treated

793 membranes.

794
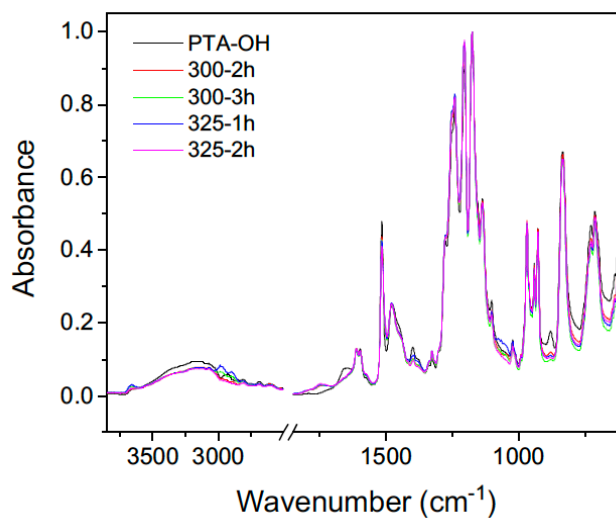
795
796 **Fig. S5.** FTIR spectra. Untreated membranes (PTA-OH) and membranes treated at different

797 temperatures and times.

798

799
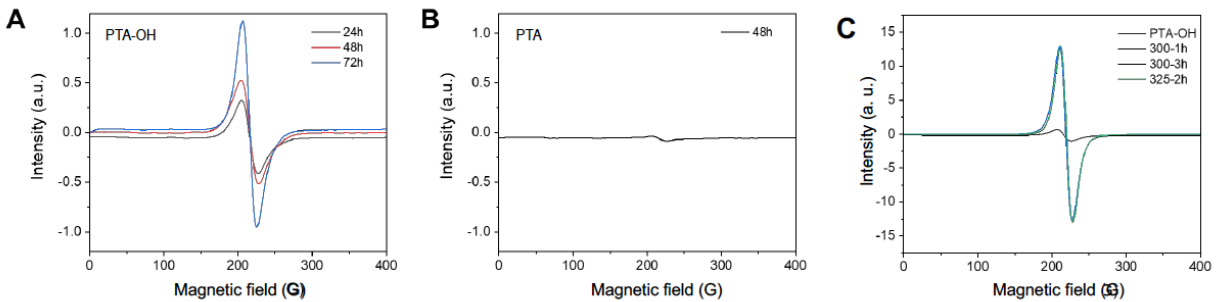
Fig. S6. EPR spectra. (A, C) PTA-OH and (B) PTA obtained by reacting polyoxadiazole at 195°C with (A, C) aminophenol or (B) aniline. Reaction times: (A) 24, 48, 72h, (B) 48h and (C) 24h. (C) PTA-OH was further treated at 300 and 325°C for 1 to 3h.
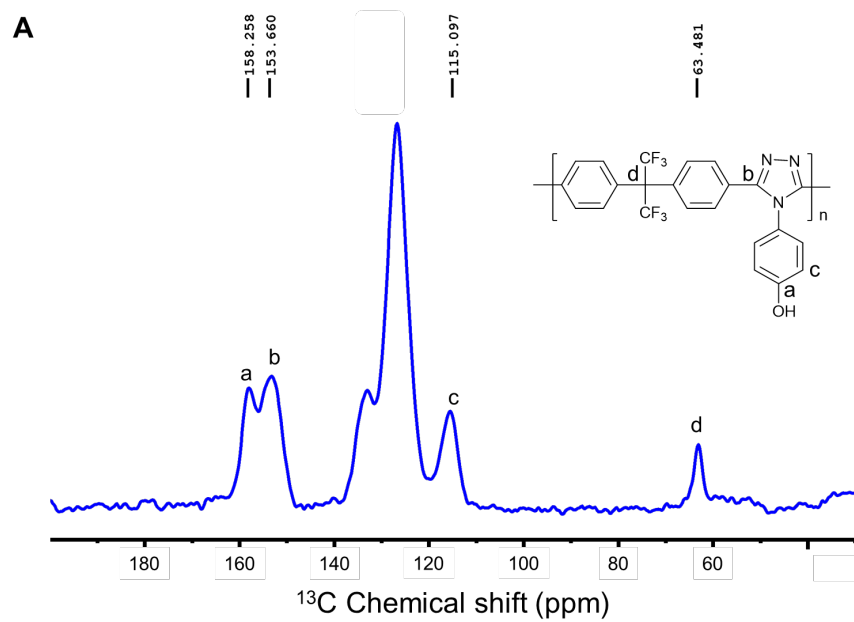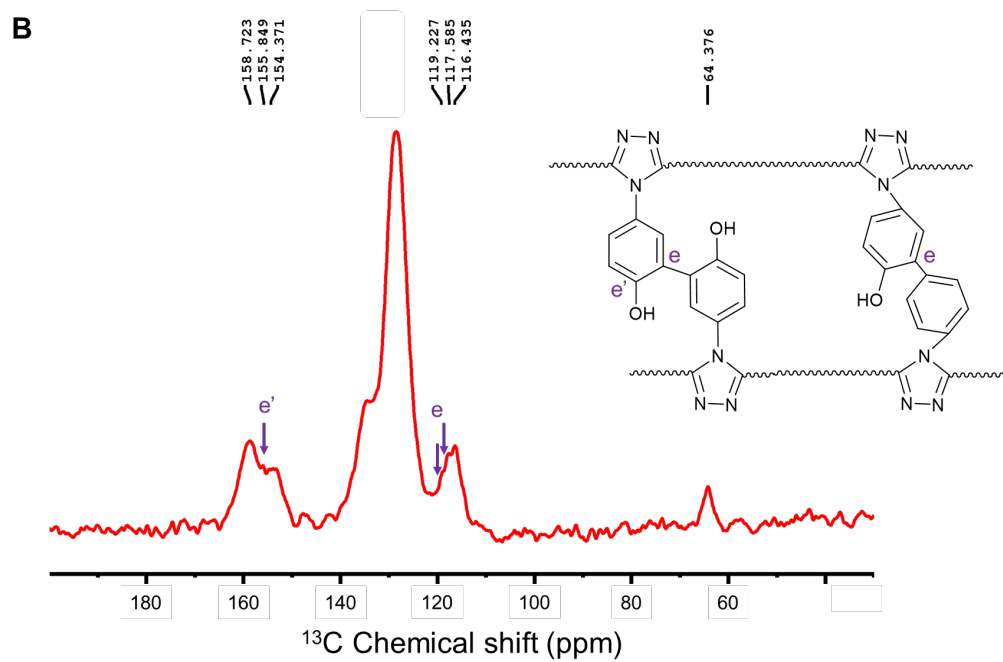
Fig. S7. ^{13}C solid-state NMR (CP MAS) spectra. (A) untreated PTA-OH membranes and (B) treated at 325°C for 2h (D325-2h).
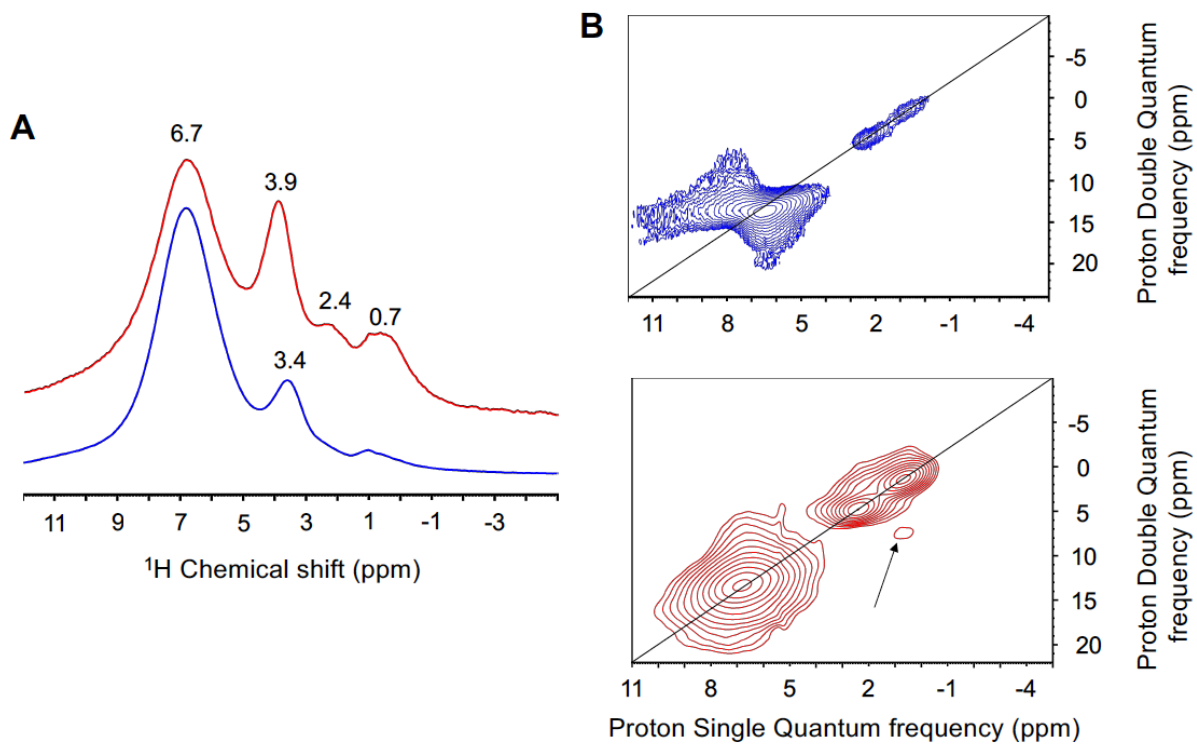
Fig. S8. ^{1}H solid-state and 2D ^{1}H-^{1}H quantum NMR spectra. (A) ^{1}H solid-state MAS NMR and (B) 2D ^{1}H-^{1}H double quantum/single quantum spectra of untreated PTA-OH membranes (blue line) and of D325-2h membranes.

821
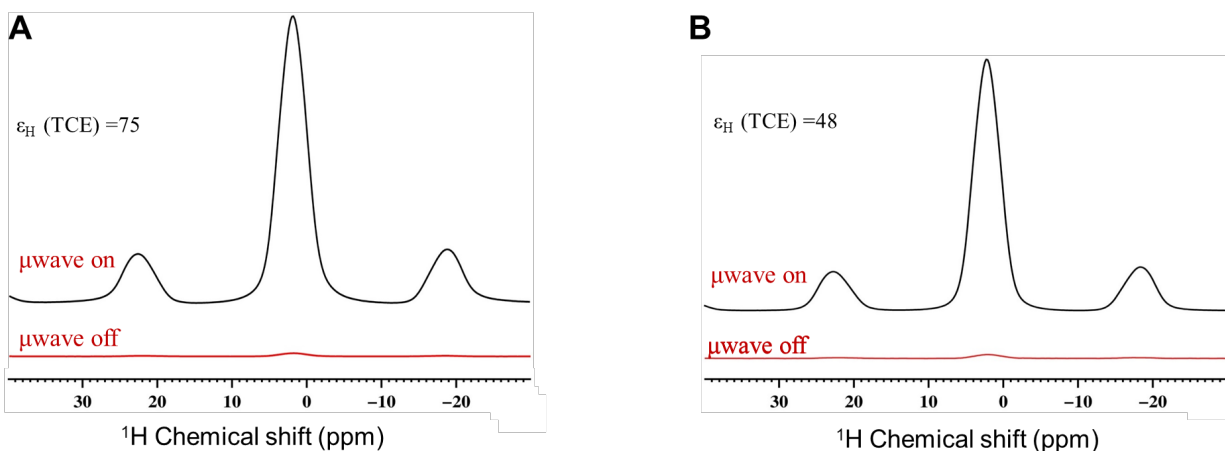
822

823

824 **Fig. S9.** ^{1}H MAS DNP SENS (100 K, 400 MHz / 263 GHz). (A) untreated PTA-OH and (B) D325-

825 2h membrane in a 16 mM TEKPol solution in 1,1,2,2-tetracholoethane (TCE). The recycle delay

826 was 3 s, and the MAS frequency was 8 kHz (ε = DNP enhancement factor). The sample was stored

827 in its rotor at -4 ℃. Red line represents the spectra without any microwave irradiation (16 scans),

828 while the black line shows the experiment under microwave irradiation (16 scans).

829

830

831
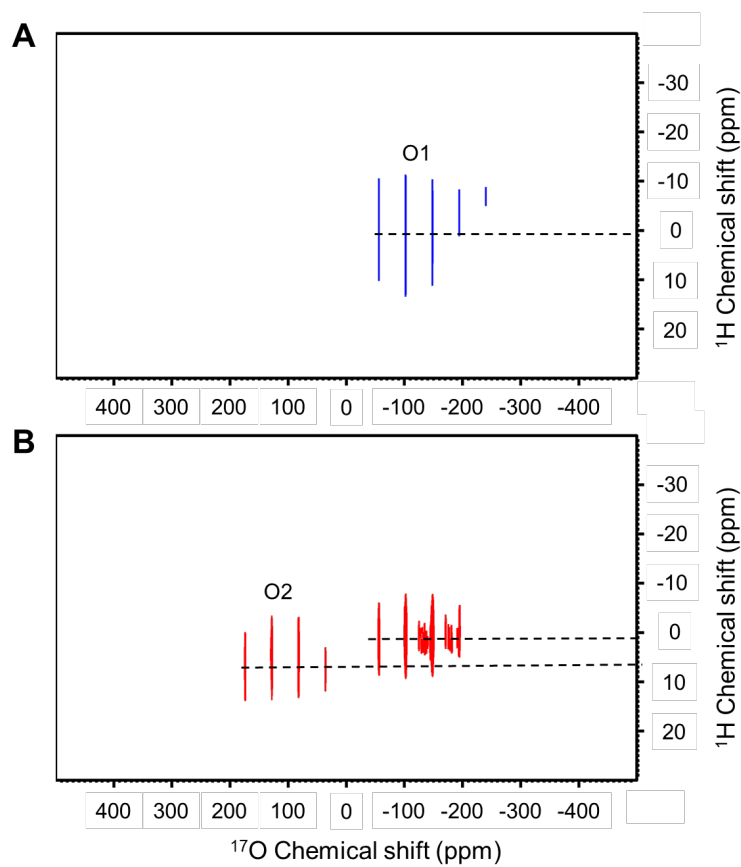
Fig. S10. $^{17}O\{1H\}$ PRESTO-QCPMG HETCOR DNP spectra. (A) untreated PTA-OH and (B) treated membrane at 325°C for 2h (D325-2h).

A

839

B

840

841
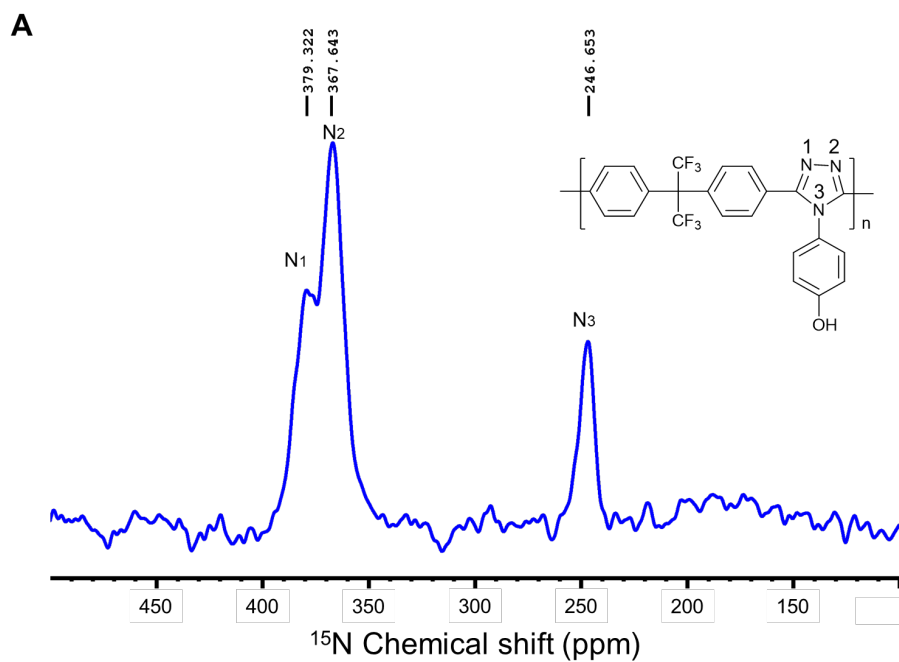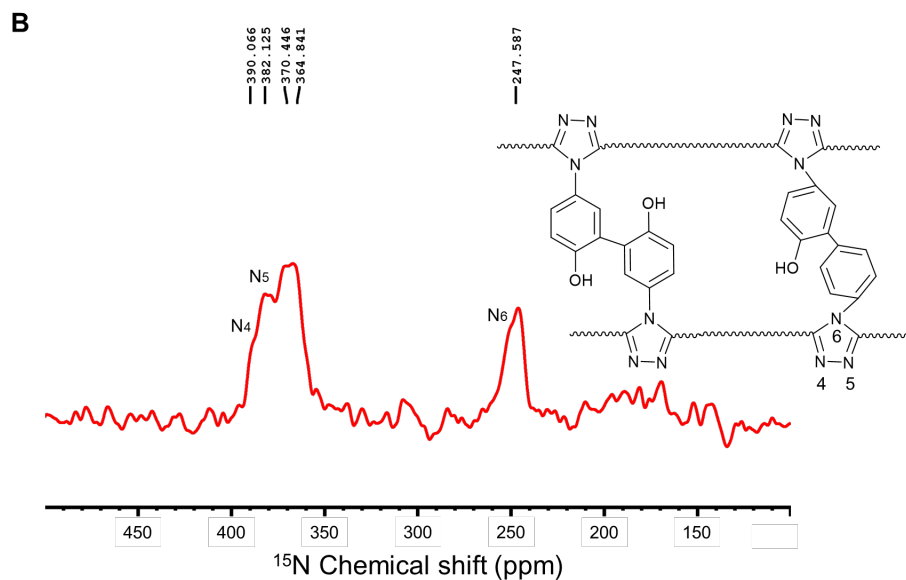
Fig. S11. 1D ^{1}H–^{15}N cross-polarization magic-angle spinning (MAS) DNP SENS spectra. (A) untreated and (B) treated membrane in a 16 mM TEKPol solution in 1,1,2,2-tetrachloroethane (TCE).

845

846
847
848
849

850
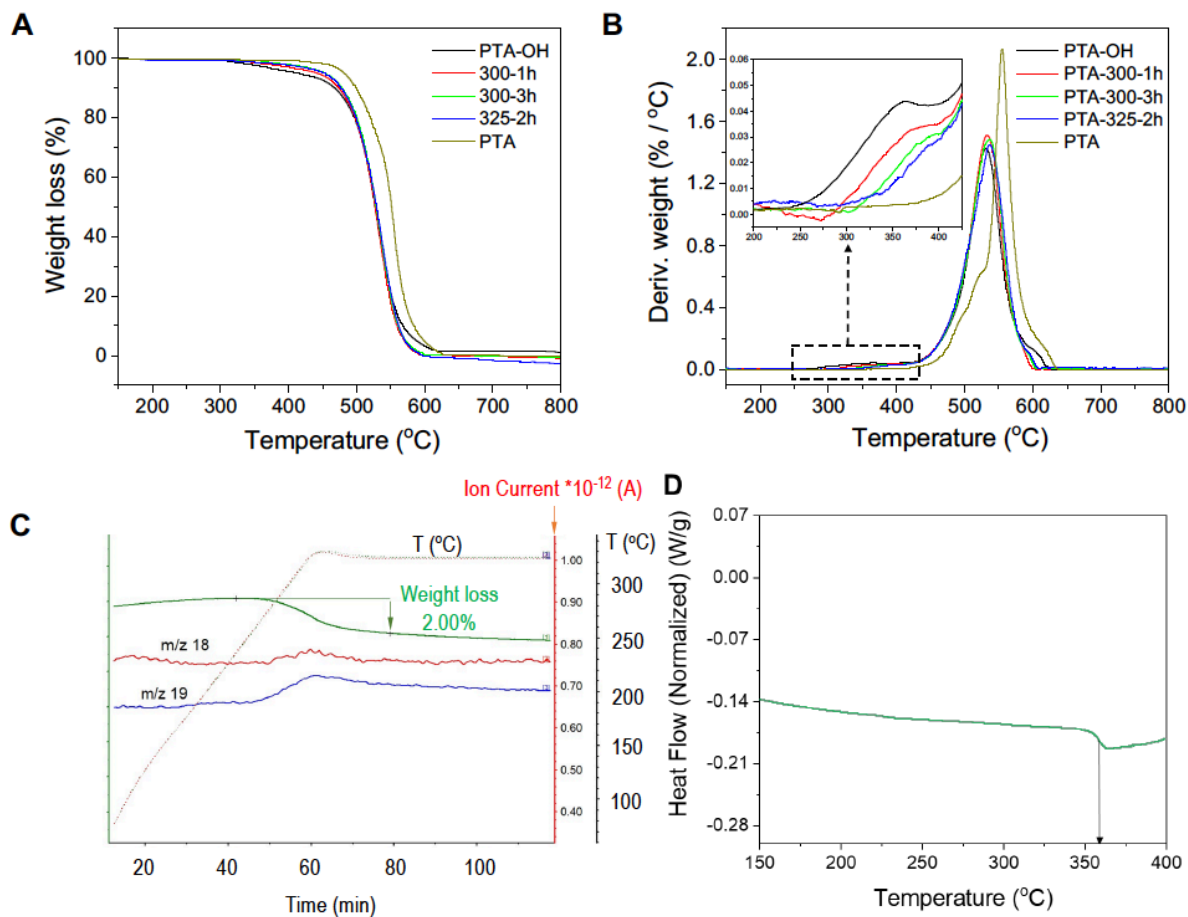
Fig. S12. Thermal analysis of PTA and PTA-OH membranes. Membranes prepared without or with treatment at different temperatures and time: (A) weight loss as a function of temperature and (B) corresponding curves derivative; (C) TGA-MS data for a PTA-OH sample heated to 325℃, under a heating rate of 5 °C min^{-1}. After reaching the temperature, the sample was kept under this condition for 1h. (D) DSC, second heating curve.

856
857
858
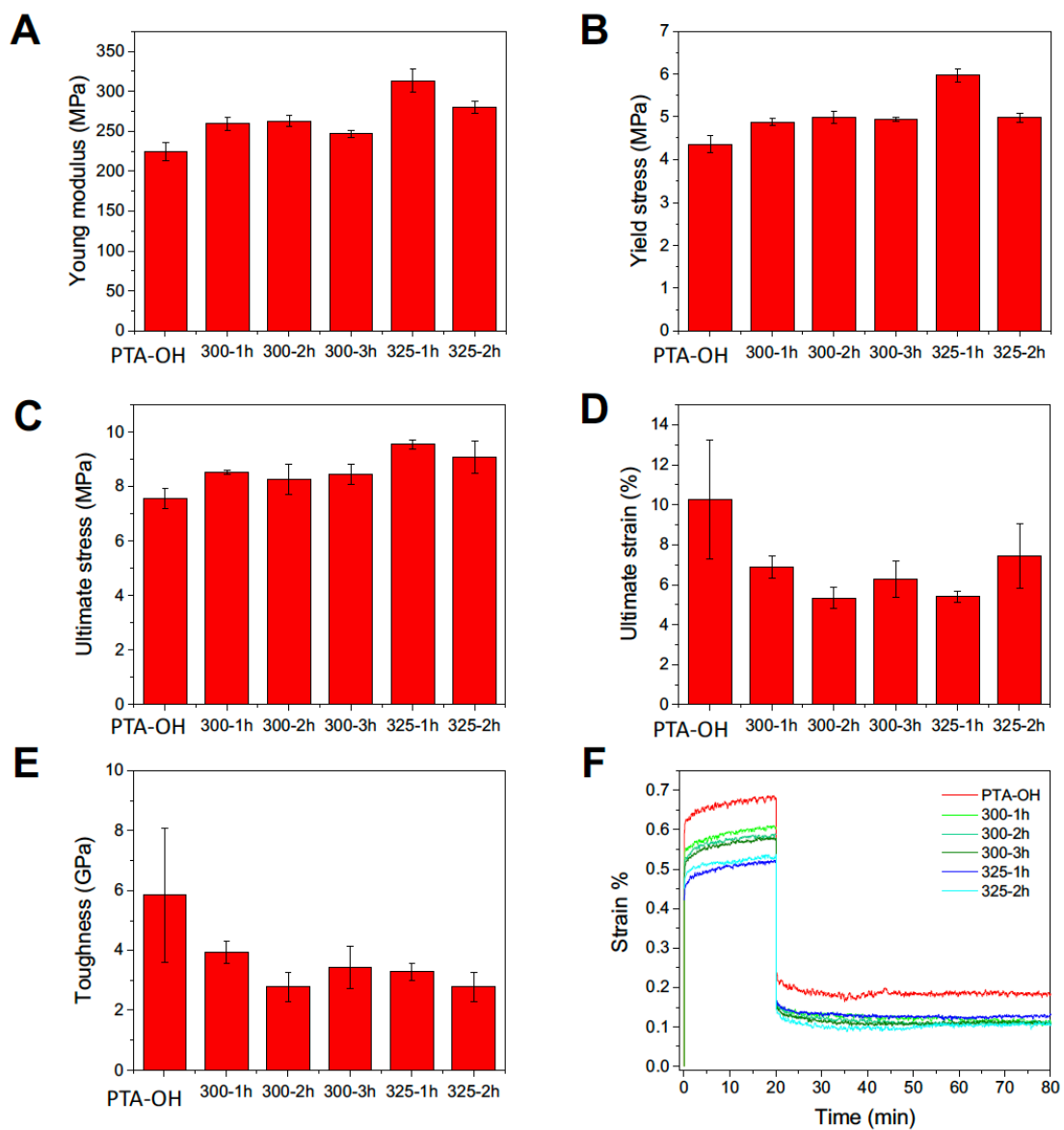
859

860 **Fig. S13.** Mechanical properties of the membranes before and after the thermal treatment. (A)

861 Young's modulus, (B) yield stress, (C) ultimate stress, (D) ultimate strain, and (E) toughness, (F)
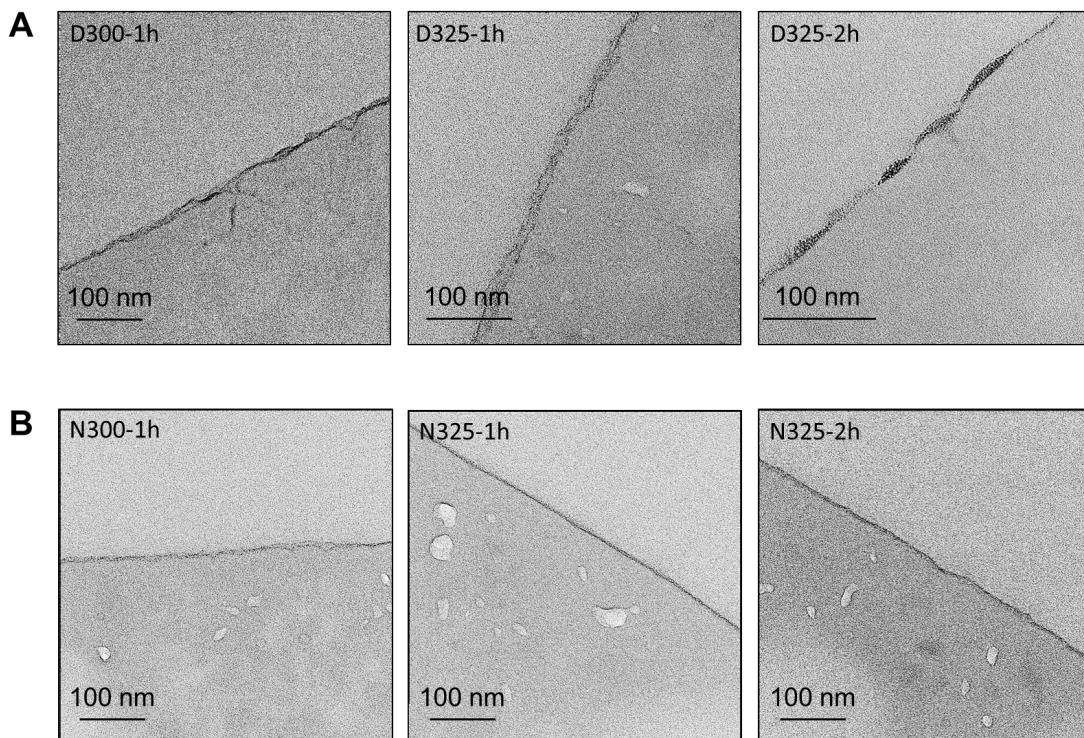
862 creep-recovery curves.

863

864
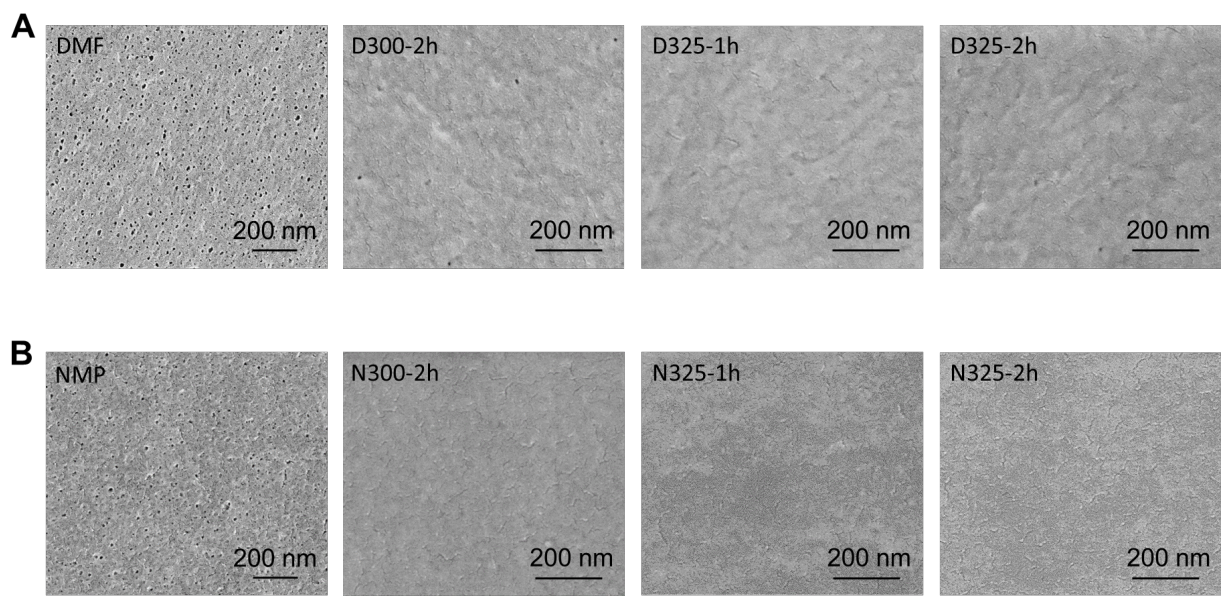
Fig. S14. SEM images of membrane surfaces. PTA-OH membranes cast from solutions in (A) DMF and (B) NMP without and with thermal treatment.
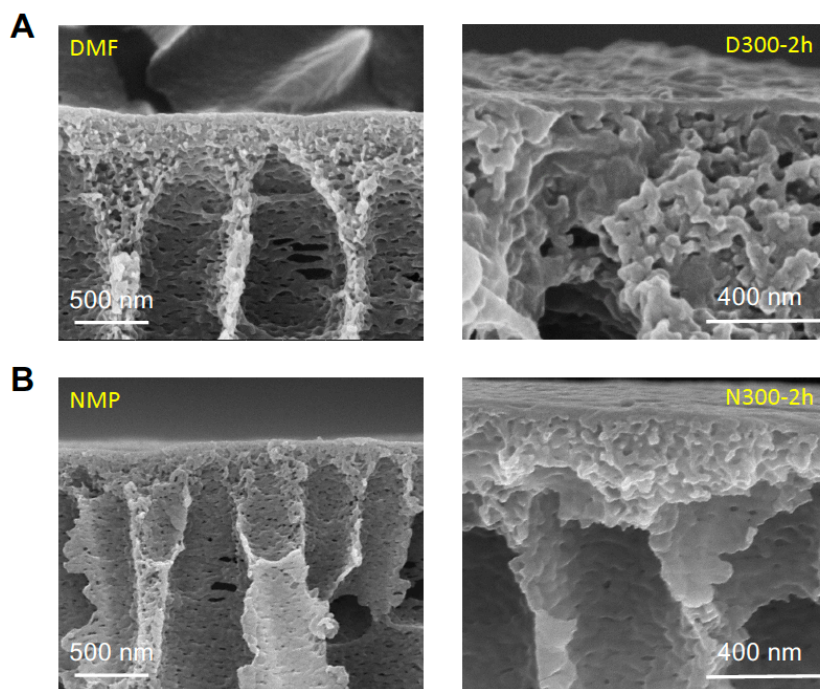
Fig. S15. SEM images of membrane cross-sections. PTA-OH membranes cast from solutions in (A) DMF and (B) NMP without and with thermal treatment.
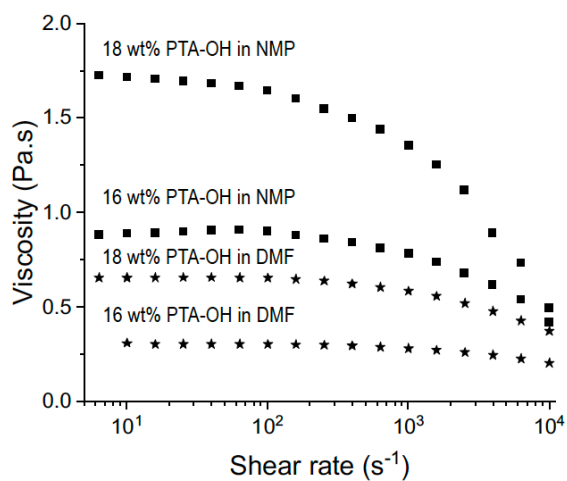
Fig. S16. TEM images of ultramicrotomed membranes. PTA-OH membranes cast from solutions in (A) DMF and (B) NMP after thermal treatment.
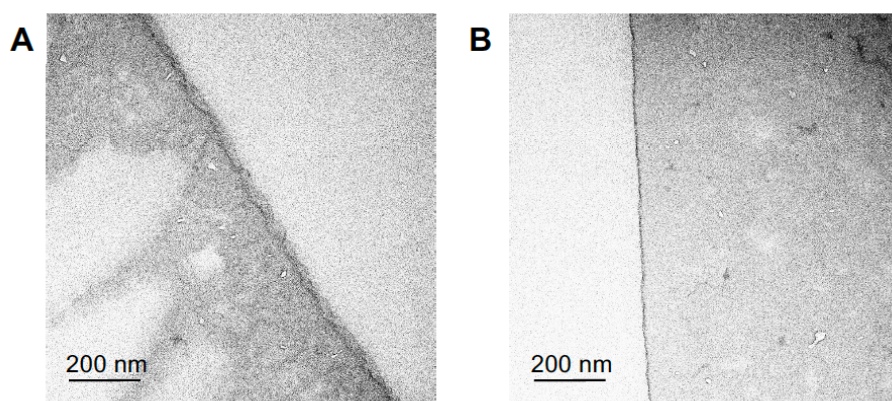
Fig. S17. TEM images of ultramicrotomed membranes. Membranes treated at 325°C for 2h, which were obtained starting from (A) 16 wt% and (B) 18 wt% PTA-OH solutions in DMF.

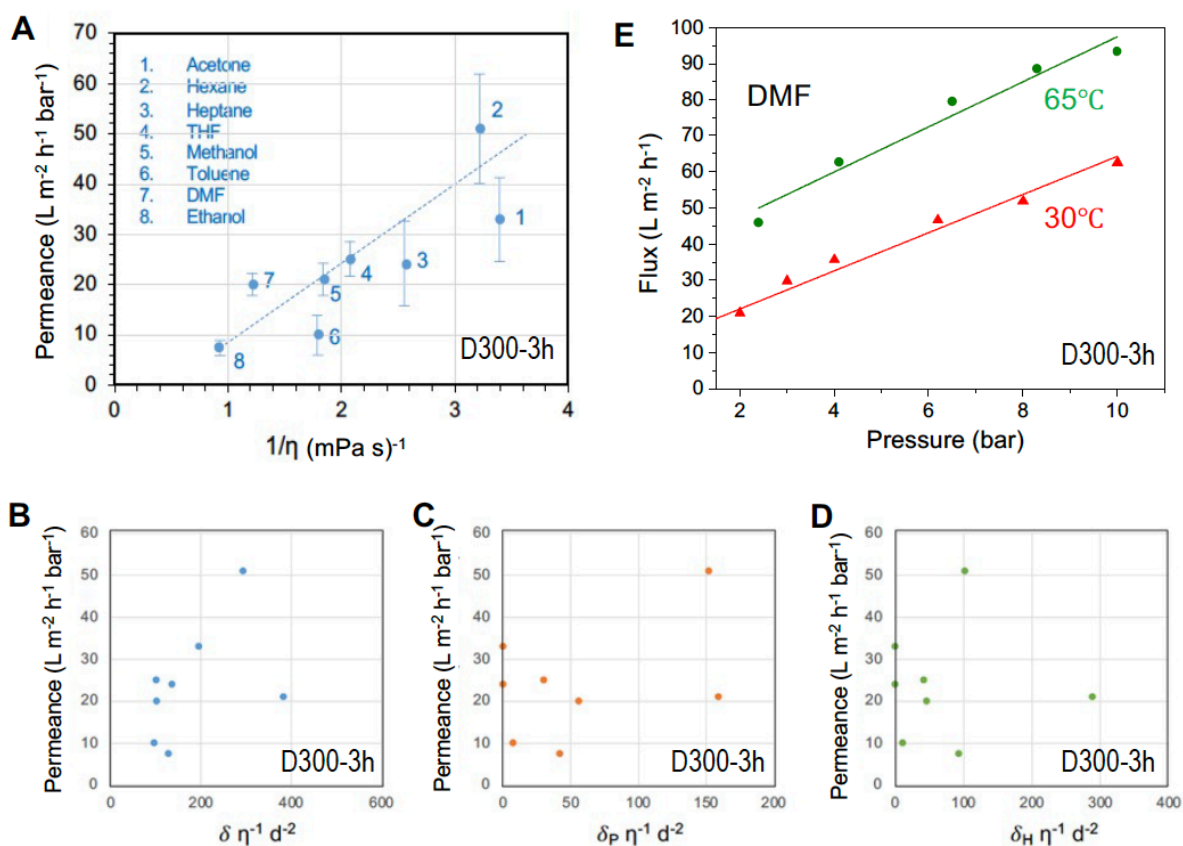**Fig. S18.** Rheology of the membrane casting solutions. Viscosity of solutions of 16 and 18 wt% PTA-OH versus shear rate.

889

890

891

892 **Fig. S19.** Organic solvent permeances through D300-3h membranes. (A) Permeances of different

893 solvents as a function of the inverse of their viscosities. (B, C, D) Solvent permeances correlated

894 with Hansen solubility parameters, as a function of the inverse of their viscosity, multiplied by the

895 inverse of the molecular diameters and Hansen solubility parameters. (B) total (δ), (C) polar (δ_P)

896 and (D) H-bonding (δ_H) contributions. Units: δ, $MPa^{1/2}$, η, mPa s, and d, nm; (E) DMF flux as a

897 function of pressure.

898

899
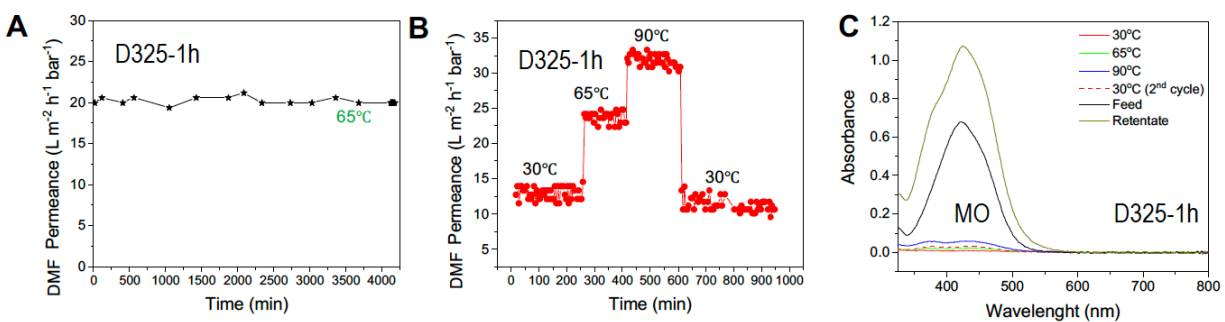
Fig. S20. Performance stability for D325-1h membranes. (A) Permeance as a function of time. (B) Performance in sequential changes of temperature. (C) Methyl Orange (MO) rejection in sequential temperature changes (absorbances of the permeates collected at 30, 65 and 90°C, feed and retentate).
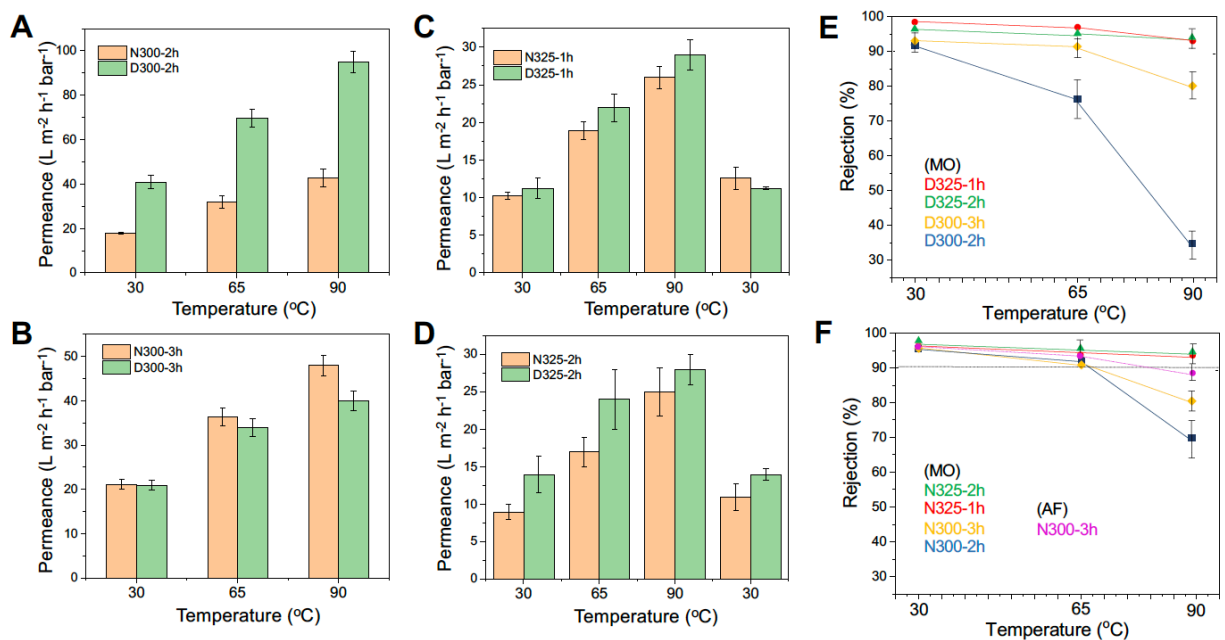
Fig. S21. Filtration of MO solutions in DMF at different temperatures. Permeances of membranes cast from PTA-OH solutions in NMP (orange) or DMF (green) treated under different conditions: (A) N300-2h and D300-2h (B) N300-3h and D300-3h, (C) N325-1h and D325-1h (D) N325-2h and D325-2h. (E) MO rejection as a function of temperature for D300-2h, D300-3h, D325-1h, D325-2h membranes. (F) MO rejection as a function of temperature for analogous membranes cast from solutions in NMP; AF rejection for N300-3h.
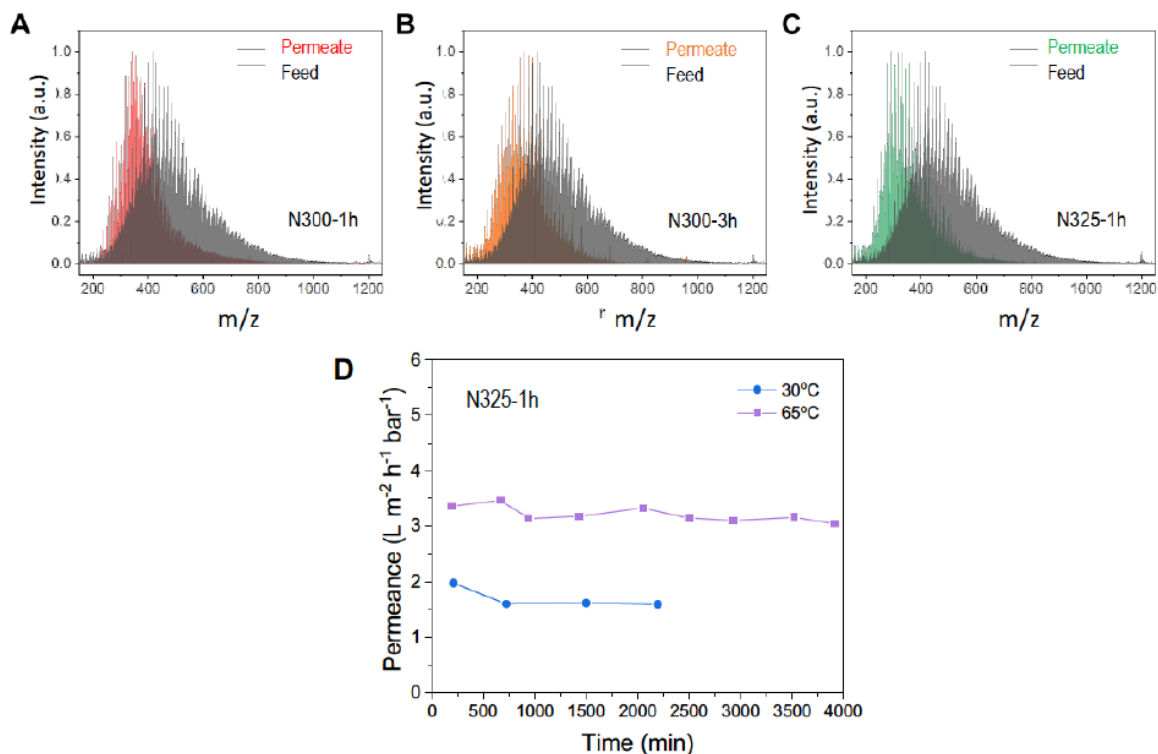
913
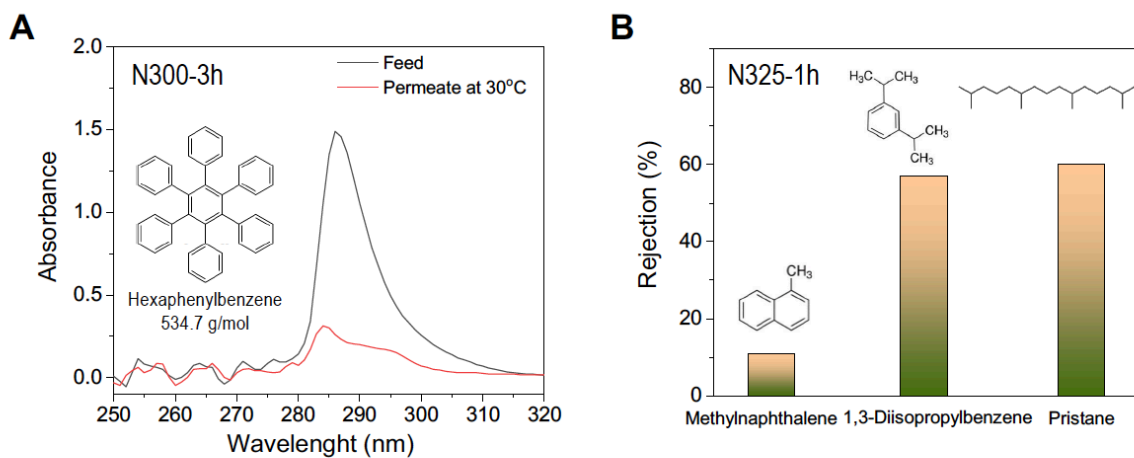
914

915 **Fig. S22.** Membrane separation performances using hydrocarbons solutions in toluene. (A) UV-
916 Viz spectra of feed (hexaphenylbenzene solution) and permeate using N300-3h membranes. (B)
917 Rejection of multicomponent hydrocarbons using N325-1h membranes.

918
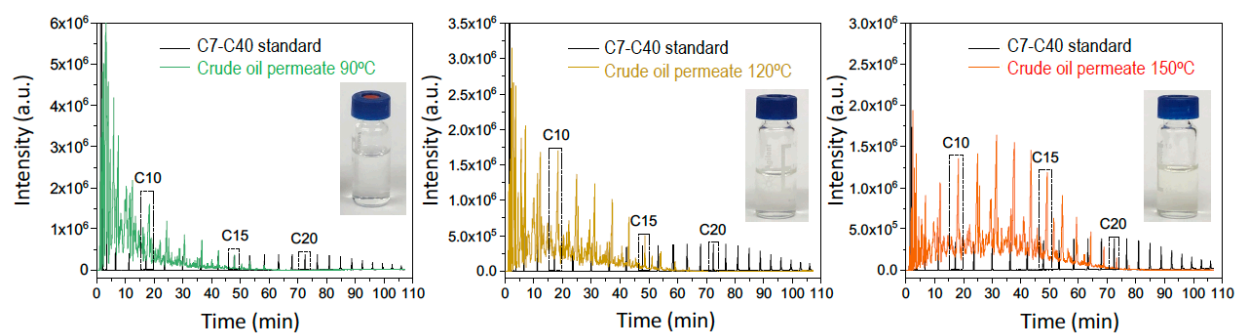
919

920

Fig. S23. Dilute crude-oil separation using ultrathin PTA-OH membranes. (A, B, C) FT-ICR MS spectra of the feed and permeates filtered at 65°C using N300-1h, N300-3h and N325-1h membranes. The feed consists of Arabian light 1:40 (volume ratio) crude oil:toluene. (D) Permeance of dilute crude oil solutions at 30 °C and 65 °C using N325-1h membranes.

925

Fig. S24. Gas chromatograms of different crude oil permeate fractions. Fractions collected after filtration with N300-1h membranes at 90°C, 120°C, and 150°C, respectively, compared to those of C_7-C_{40} normal- alkanes standard solutions in hexane. The inset photographs show the permeate obtained at each filtration temperature.
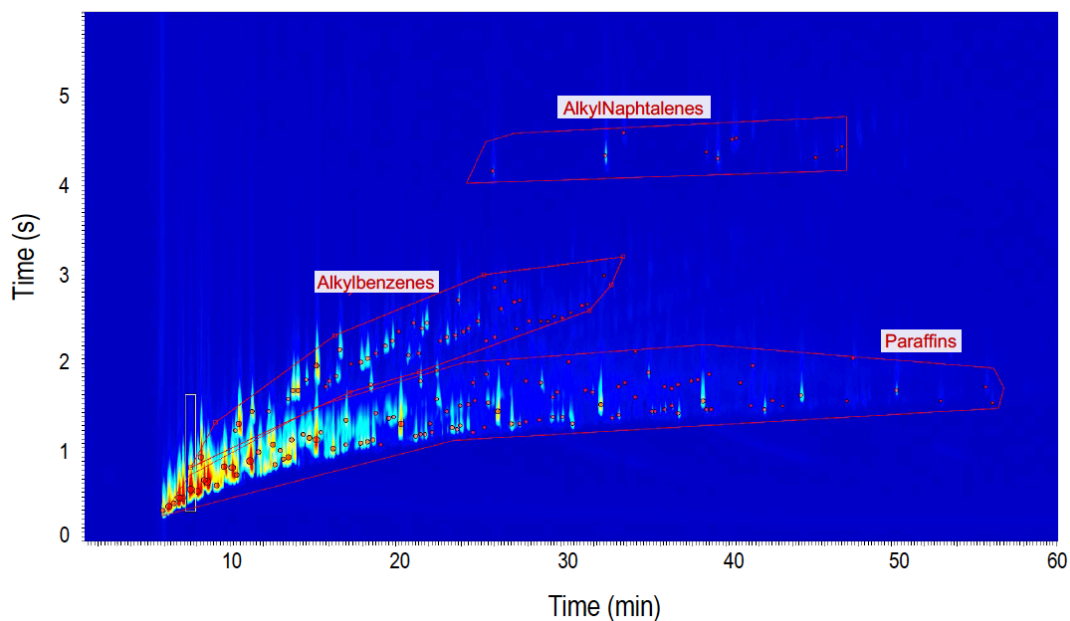
Fig. S25. Two-dimensional (2D) gas chromatogram (GCxGC). Permeate obtained using a N300-1h membrane after filtration of crude oil at 90°C. Paraffins and isoparaffins are preferentially concentrated. Light alkylbenzenes hydrocarbons were also detected.

Table S1. Summary of ultrathin polytriazole membranes performances.

Membrane (Material)	Permeance (L m^{-2} h^{-1} bar^{-1}) DMF (T)	toluene	Solute	MW (g mol^{-1})	Rejection (%)	Ref.
PTA-OH Membranes						
D300-3h (PTA-OH)	21 (30°C)	10	Methyl orange	327	93 (DMF)	This work
N300-3h (PTA-OH)	21 (30°C)		Methyl orange	327	95	This work
	36 (65°C)		Methyl orange	327	90	
	48 (90°C)		Acid fuchsin	585.5	88	
Commercial Membranes						
Starmem 122® (PI)	-	1.37	Sudan 408	464	78.7	(21-23)
	-	0.56	PS oligomers	270	90	
PuraMem 280 (PI)	-	0.67	PS oligomers	280	90	(24)
PuraMem S600 (PI)	-	2	Palladium (II) acetate	224	60	
Starmem® 240 (PI)	-	0.7	PS oligomers		90	(25)
Duramem300 (PI)	0.26 (30°C)					(10)
	0.05 (85°C)					
PERVAP4060 (PDMS)	-	2.2	Tetraoctyl ammonium bromide	546	92.5	(26)
Integral Asymmetric Membranes						
PEG400/ Matrimide5218 (PI)	10.8		Rose Bengal	1017	72.53	(27)
PBI-based	10.49		Tetracycline	444	66	(28)
PBI-based	0.6 (30°C)					(10)
	1.7 (85°C)					
PEEK	0.05 (30°C)					(10)
	0.2 (85°C)					
TFC Membranes						
Membrane (Material)	Permeance (L m^{-2} h^{-1} bar^{-1}) DMF (T)	toluene	Solute	MW (g mol^{-1})	Rejection (%)	Ref.
Polyarylate/ PI support		2.5	crystal violet	408	99 (MeOH)	(29)
PA/PI support or alumina		0.18	Methyl orange	327	97.7 (MeOH)	(30)
PA/PI support or alumina		0.1	Methyl orange	327	96.8 (MeOH)	
PA/PI support or alumina		3.45	Methyl orange	327	98.9 (MeOH)	
PA	8 (30°C)		PS oligomers	600	90	(31)
	10 (60°C)		PS oligomers	600	90	
	12 (90°C)		PS oligomers	600	90	
CD-based		1.6	Methyl orange	327	93 (MeOH)	(32)

CD-based	1	-	Methyl orange	327	95.7 (EtOH)	(33)
CD-based		19.8	Methyl orange	327	88 (MeOH)	(34)
Trianglamine/ PAN support		35.5	Orange G	452.4	91 (MeOH)	(35)
Spirocyclic polymers		0.1-07	Polystyrene, dilute hydrocarbons, crude oil	335	>90 (toluene)	(12)
COF		7.8	Sudan black B	456	99	(36)
COF		5.3	Sudan black B	456	98	(36)
COF	5.5		Rose Bengal	1017	99.5	(37)
COF	8.1		Brilliant blue	826	94.8 (EtOH)	(38)

945 PI = polyimide, PA = polyamide, PDMS = polydimethylsiloxane, PBI = polybenzimidazole, PEEK =

946 polyetheretherketone, COF = covalent organic framework, CD = cyclodextrin, PAN = polyacrylonitrile

947

948